22. A GEOTHERMAL AND GEOPHYSICAL SURVEY ON THE SOUTH FLANK OF THE COSTA RICA RIFT: SITES 504 AND 505[1]

Michael A. Hobart, Marcus G. Langseth, and Roger N. Anderson, Lamont-Doherty Geological Observatory[2]

ABSTRACT

A detailed geothermal and geophysical survey was carried out on the south flank of the Costa Rica Rift, in the eastern Pacific Ocean, to select the locations for Deep Sea Drilling Project Sites 501/504 and 505. The area surveyed was approximately one degree square, spanning crust ranging in age from 4 to 6 Ma.

The younger crust near Site 505 consists of typical abyssal hills with thin sediment cover and numerous basement outcrops along fault scarps. Heat flow is low and highly variable, indicating extensive advective heat transfer from the crust to the ocean. Seismic velocities in Layer 2A are low. A major east-west-trending trough with several hundred meters of relief is present in the northern part of the survey area. Hole 505 is located in sediments along the bottom of this trough. We reinterpret a focal plane solution published by Molnar and Sykes (1969) that indicates that left-lateral strike-slip motion is occurring along this trough, instead of on a north-south fracture zone, as they believed. We infer from this solution that this trough may well be the site of intraplate deformation associated with the continuing collision of the Galapagos Spreading Center system and Central America. The trough may be the location of a potential ridge jump to the south from the current Costa Rica Rift axis.

The older oceanic crust near Sites 501/504 has a 200–300-m-thick sediment cover draped over basement. This area has very few areas of exposed basement. Heat flow is high, at values predicted by plate cooling models, and the variability of the heat flow is less than that observed in the younger crust. Seismic velocities in Layer 2A are higher than in the younger crust. The average velocity profile determined from combining several sonobuoy solutions is very similar to that determined by the Oblique Seismic Experiment carried out in Hole 504B (Stephen, 1983). The transition from low heat flow in the younger crust to high heat flow in the older crust can be closely matched by a model of the reheating of a layer initially cooled by circulating seawater. The best match occurs when the thickness of the cooled layer is about 6 km. This suggests that occasional structurally controlled fault zones of high permeability may play a major role in the early thermal history of the oceanic crust.

INTRODUCTION

The international phase of the Deep Sea Drilling Project (IPOD) has had deep sampling of the ocean crust as one of its main objectives for several years. This objective has proven to be somewhat elusive. Shallow areas that are easily within the reach of the *Glomar Challenger*'s drill string are usually areas of young oceanic crust which are highly fractured and are quite difficult to drill (e.g., Hekinian, Rosendahl, et al., 1980). Areas that are more easily drilled because of greater cementation of the fractures in the uppermost crust are usually older and in much deeper water, increasing the operational difficulties (e.g., Sites 417 and 418, Donnelly, Francheteau, Bryan, Robinson, Flower, Salisbury, et al., 1980).

The regional patterns of heat flow on the flanks of mid-ocean ridges have been the object of intensive study in recent years (Anderson and Hobart, 1976; Anderson et al., 1977; Herman et al., 1977; Hobart et al., in press). These studies have shown a consistent pattern. The heat flow is very low in young crust, much below that predicted by plate cooling models. The heat flow increases to the values predicted by plate models at some age on the flank of the mid-ocean ridge and thereafter follows the cooling curve. The age at which this occurs varies from region to region because of varying topographic relief and rates of sedimentation.

Anderson and Hobart (1976) discovered that the Galapagos Spreading Center in the eastern equatorial Pacific had the lowest known age for the transition from subtheoretical to theoretical heat flow, about four million years. They also discovered an area of seafloor on the south flank of the Costa Rica Rift (CRR) that had smooth basement, thick and uniform sediments, and high heat flow (Fig. 1). Therefore, when an IPOD drilling program to study the Galapagos "Mounds" hydrothermal area (Klitgord and Mudie, 1974; Williams et al., 1974; Lonsdale, 1977a; Corliss et al., 1979) was proposed, they suggested that this area on the south flank of the Costa Rica Rift was a good target for drilling.

This suggestion was based on the hypothesis that the return of the heat flow to theoretical values was due to either the isolation of hydrothermal convection cells in the crust beneath the sediment cover or the stopping of the convection within the cells because metamorphic alteration sealed the fractures that permitted convection. The possibility that the sediment cover might seal off the circulation and cause an alteration of the temperature and chemistry leading to subsequent sealing was also recognized. Thus, the heat flow pattern on ridge flanks possibly was related directly to the amount of fractures and alteration in the upper crust and was, therefore, a

[1] Anderson, R. N., Honnorez, J., Becker, K., et al., *Init. Repts. DSDP*, 83: Washington (U.S. Govt. Printing Office).
[2] Address: Lamont-Doherty Geological Observatory of Columbia University, Palisades, NY 10964.

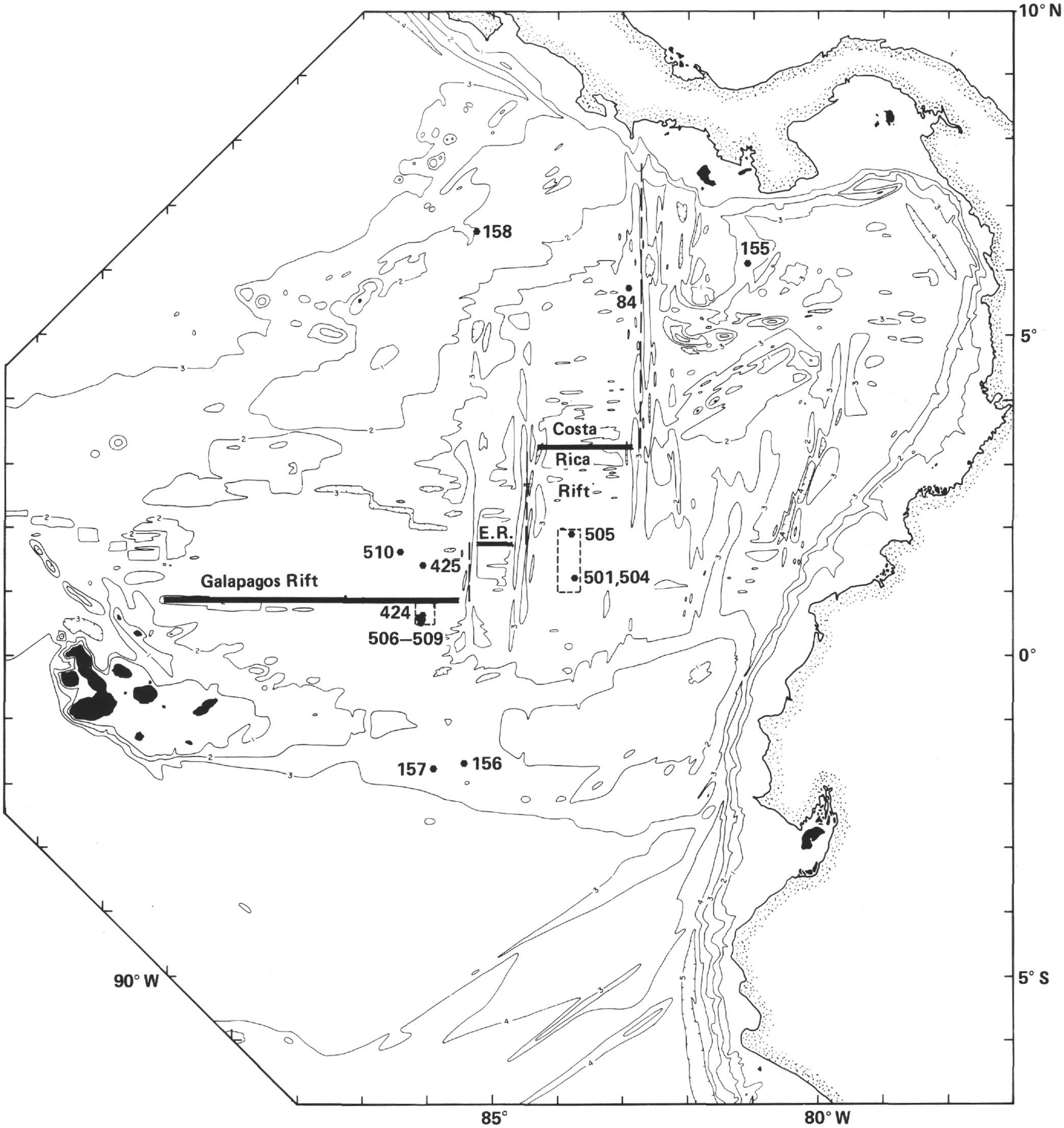

Figure 1. Bathymetric and tectonic chart of the Panama Basin (after Lonsdale and Klitgord, 1978). Contour interval 1000 m, DSDP sites from Legs 16, 54, 68, 69, 70 shown; box shows detailed survey area.

clue to drilling conditions. This was consistent with the drilling results that had been obtained by the *Challenger* up to that time.

The site on the CRR flank was the youngest area known in which these relationships could be tested and had the added advantage of being one of the few areas where a higher temperature of alteration might be expected to take place in the upper crust (on the average) because of the high theoretical heat flow of such young crust (Anderson et al., 1977).

This paper presents the results of a predrilling site survey on the flank of the Costa Rica Rift. The survey was carried out in December 1977, aboard *Robert D. Conrad*, Cruise 21-17 (Fig. 2). Additional data incorporated in this study come from *Glomar Challenger* Legs 68, 69, and 70; *Gilliss* Cruise 79-04 (R. Stephen, chief

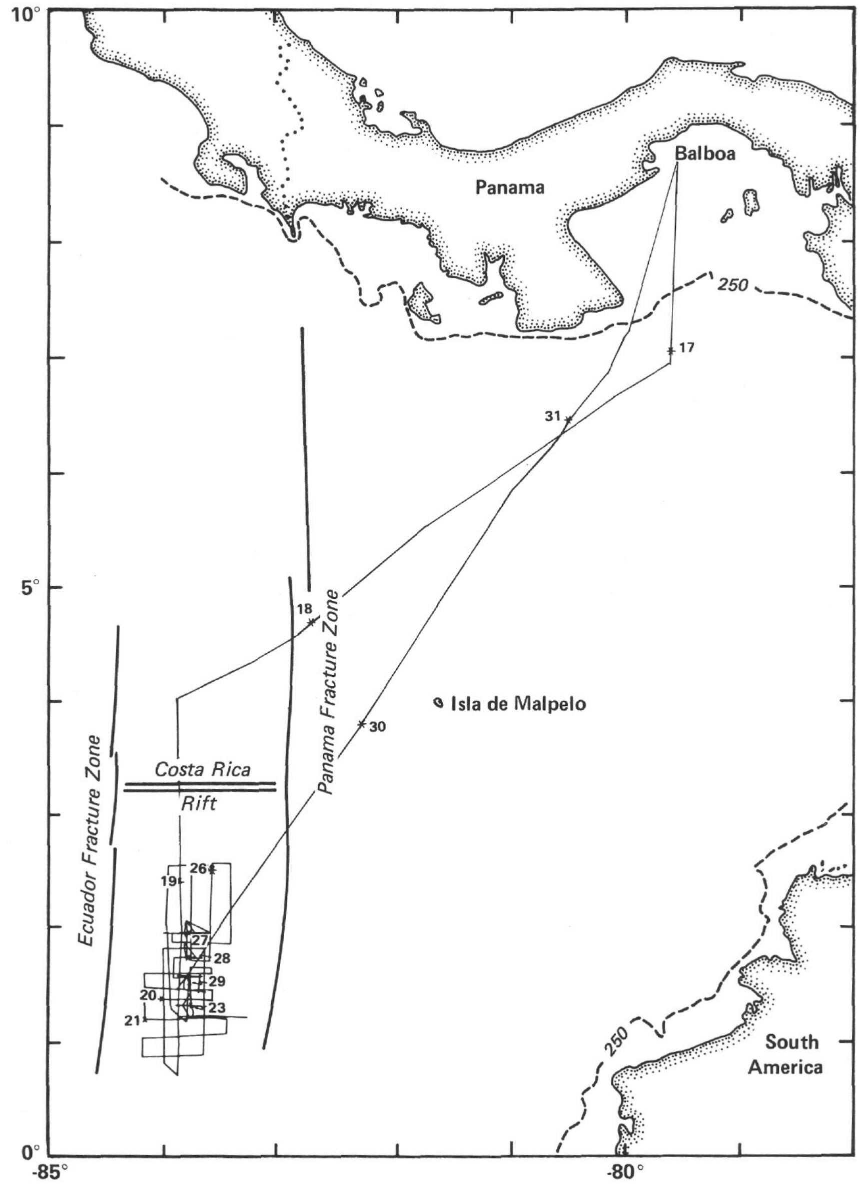

Figure 2. Overall track chart for *Robert D. Conrad* Cruise 21-17, December 1977.

scientist); *Discovery* Cruise 110 (R. C. Searle, chief scientist); and existing data from Lamont-Doherty, Scripps Institution of Oceanography, Oregon State University (van Andel et al., 1971), Hawaii Institute of Geophysics, and the National Oceanographic and Atmospheric Administration.

MAGNETIC ANOMALIES AND SPREADING HISTORY

Magnetic anomalies on the Costa Rica Rift are large in amplitude, well defined, and very linear (Fig. 3). All of the magnetic data that we have used in this study were acquired with proton precession magnetometers, and were digitized at approximately 5-min. intervals. The magnetic anomalies over the Costa Rica Rift are not so large as those over the Galapagos Rift to the west. This is presumably due to the restriction to the Galapagos Rift of the high iron-titanium basalts that have high magnetic remanence (Vogt and Johnson, 1973; Anderson et al., 1975; Vogt and de Boer, 1976). The total spreading rate of the Costa Rica Rift is approximately 72 mm/yr. (Klitgord et al., 1975; Hey et al., 1977) and is very similar to the rate on the eastern end of the Galapagos Rift (Klitgord and Mudie, 1974).

The Costa Rica Rift does differ from the Galapagos Rift in that the half rates on the two flanks of the ridge are quite different. The north flank has a rate of about 30 mm/yr. (Klitgord et al., 1975; Hey et al., 1977), whereas the south flank has a rate of 38.4 mm/yr. (Klitgord et al., 1975; this study). Figure 4 is a combined plot of the magnetics and bathymetry from *Glomar Challenger*, Leg 68, projected onto 005°, together with the sediment thickness and heat-flow data. The time scale for the Cenozoic (LaBrecque et al., 1977) is shown below it. The fit, using a uniform spreading rate of 38.4 mm/yr. is remarkably good. We have found no evidence for any sig-

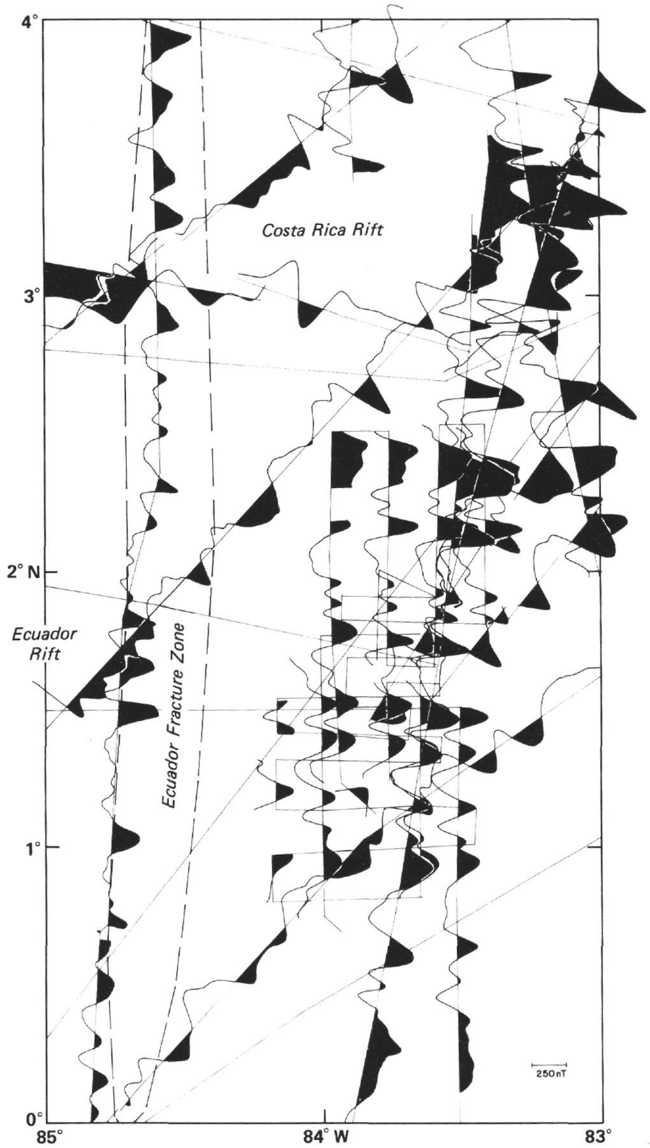

Figure 3. Magnetic anomalies plotted along track on the south flank of the Costa Rica Rift. Anomalies from normally magnetized crust in black. Because of the orientation of the spreading center and the low latitude, normal anomalies are negative.

nificant spreading-rate change out to beyond 6 Ma on the south flank. This is in contrast to Klitgord et al.'s (1975) results, but we believe that the spreading-rate change that they found was too close to the end of their data line to be easily resolved.

Klitgord et al. (1975) presented the results of a Deep Tow traverse from within our detailed survey area north across the crest of the Costa Rica Rift (Fig. 5). The upward-continued Deep Tow data agreed very well with the surface magnetics. The width of the transition zones between anomalies was 2–2.5 km, similar to that found at spreading centers on the Galapagos Rift, East Pacific Rise, and Pacific-Antarctic Rise.

These results support the hypothesis that the Costa Rica Rift is truly spreading asymmetrically, that is, if the process at the ridge crest is due to ridge-crest jumps, then they are occurring over such small distances that they are unresolvable. They must also be occurring with great regularity to preserve such consistency in spreading rates on both flanks of the ridge. It is worth noting that the fossil Malpelo Rift to the east of the Costa Rica Rift also spread asymmetrically, but that the north flank had the higher half rate. This is opposite to the situation on the Costa Rica Rift. Both of these asymmetrically spreading ridges are in contrast to the style of spreading of the Galapagos Rift segment, where the ridge crest jumps to the south, causing a net accretion of extra crust to the northern (Cocos) plate (Hey 1977; Hey et al., 1977; Anderson et al., 1976; Anderson and Hobart, 1976).

The short time interval in which the *Conrad* 21-17 detailed survey was carried out and the reasonable, though not large, distance from the magnetic equator permit us to construct a magnetic anomaly contour chart (Fig. 6). We have limited ourselves to this data set to avoid the problems from the lack of time-varying terms in the geomagnetic field models. The linearity of the anomalies is striking but it is also apparent that the blocky nature of the eruptive centers on mid-ocean ridges does have an effect. There are some distinct smaller-scale anomalies and there is also a variation in the clarity of expression in the larger "geomagnetic time scale" anomalies.

The magnetic anomaly map (Fig. 6) permits us to date Site 505 and Sites 501/504 rather closely. Site 505 is quite close to the midpoint of a narrow positive anomaly. This corresponds to the reversely magnetized interval from 4.10–4.24 Ma (LaBrecque et al., 1977), so we may assign Site 505 an age of 4.17 Ma. Similarly, Sites 501/504 are about 70% of the way across the positive anomaly corresponding to the 5.62–6.06 Ma reversal, so they have an age of about 5.93 Ma.

Additional work on the details of the magnetic-anomaly pattern and the spreading history of the Costa Rica Rift is in progress.

BATHYMETRY

A bathymetric map of the survey area on the south flank of the Costa Rica Rift has been constructed (Fig. 7). The data consist of 3.5-kHz and 12-kHz precision depth soundings and have been corrected for the variation in the velocity of sound in water. The primary sources of data for this compilation are the *Conrad* 21-17, *Gilliss* 79-04, *Glomar Challenger* 68, 69, and 70 cruises. All available existing data for this area (primarily from Lamont-Doherty and the Scripps Institution of Oceanography) have been incorporated in this figure and are shown in the track chart (Fig. 8).

The topography is strikingly oriented east–west, parallel to the spreading center. There are several distinct morphologic zones in this area. North of our survey, and extending just into the northern edge of it, is an area of typical abyssal hills of about 200 m relief. A prominent narrow ridge and broad trough (south of the ridge) extend east–west across the survey area between 2°00′N and 1°53′N. This combined ridge and trough continues to both the east and west of our survey area and probably extends all the way across the width of the

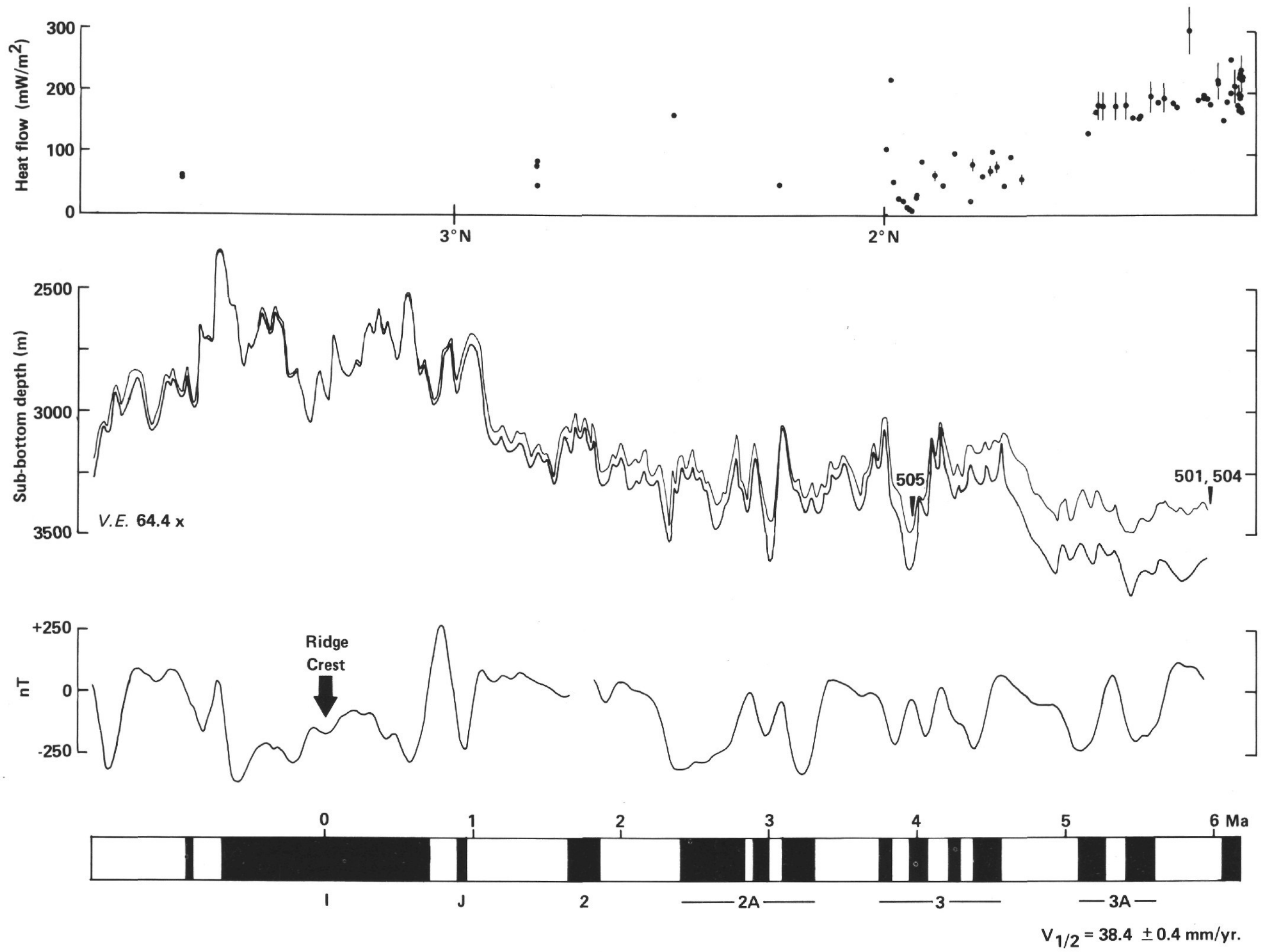

Figure 4. Combined geophysical profile over the south flank of the Costa Rica Rift. Underway data from *Glomar Challenger* Leg 68, heat flow from Anderson and Hobart (1976) and this chapter. Sites 501, 504, 505 shown.

south flank of the Costa Rica Rift. The ridge has 200–500 m relief above the seafloor to the north of it and 400–800 m relief above the trough to the south. The trough is fairly narrow in the west, about 8–10 km, but distinctly widens at 83°35′W to about 16 km in the east. The trough is bounded on the south by a broad ridge about 30 km wide with a crest 200–400 m above the trough. Superimposed on these broad features is roughness on the scale of a few kilometers. This roughness is due to many small, slightly tilted fault blocks. The steeper slopes on these blocks almost invariably face to the north and they show relief of 50–200 m. The scale of the faulting seen here is very similar to that seen to the west on the Galapagos Spreading Center. There, Deep Tow surveys (Klitgord and Mudie, 1974; Lonsdale, 1977a) and multibeam echo-sounding surveys from surface ships (Allmendinger and Riis, 1979) have shown that there are many small, tilted fault blocks from 2–4 km wide. The small-scale fault-block structure shows up well on the South Tow 6 Deep Tow profile of Klitgord et al. (1975) (Fig. 5). We will discuss this structure further when we consider the role of basement outcrops and the geothermal regime.

Moving to the south, as we proceed across the broad rise the bathymetric relief decreases as increasing amounts of sediment drape and smooth the abyssal hills. South of about 1°35′N the surface relief decreases to about 50 m. A broad low, defined by the 3500 m contour, occurs near 1°24′N. A few kilometers south of that low the small-scale relief increases to about 100 m amplitude. Near Sites 501/504 the topography shows clear east-west-aligned ridges a kilometer or two wide. Stephen (1983) has a contour map of the immediate vicinity of Sites 501/504 which differs somewhat from our Figure 7. This is due to a somewhat different contouring philosophy used by Stephen, his primary reliance on the *Gilliss* 79-04 data, and his use of a 50-m contour interval.

A larger hill, with 200–250 m relief, is found at about 1°00′N. The north face of this east-west hill has a prominent scarp with exposed basement, especially at the eastern end near 83°30′W. This exposure is, we believe, the

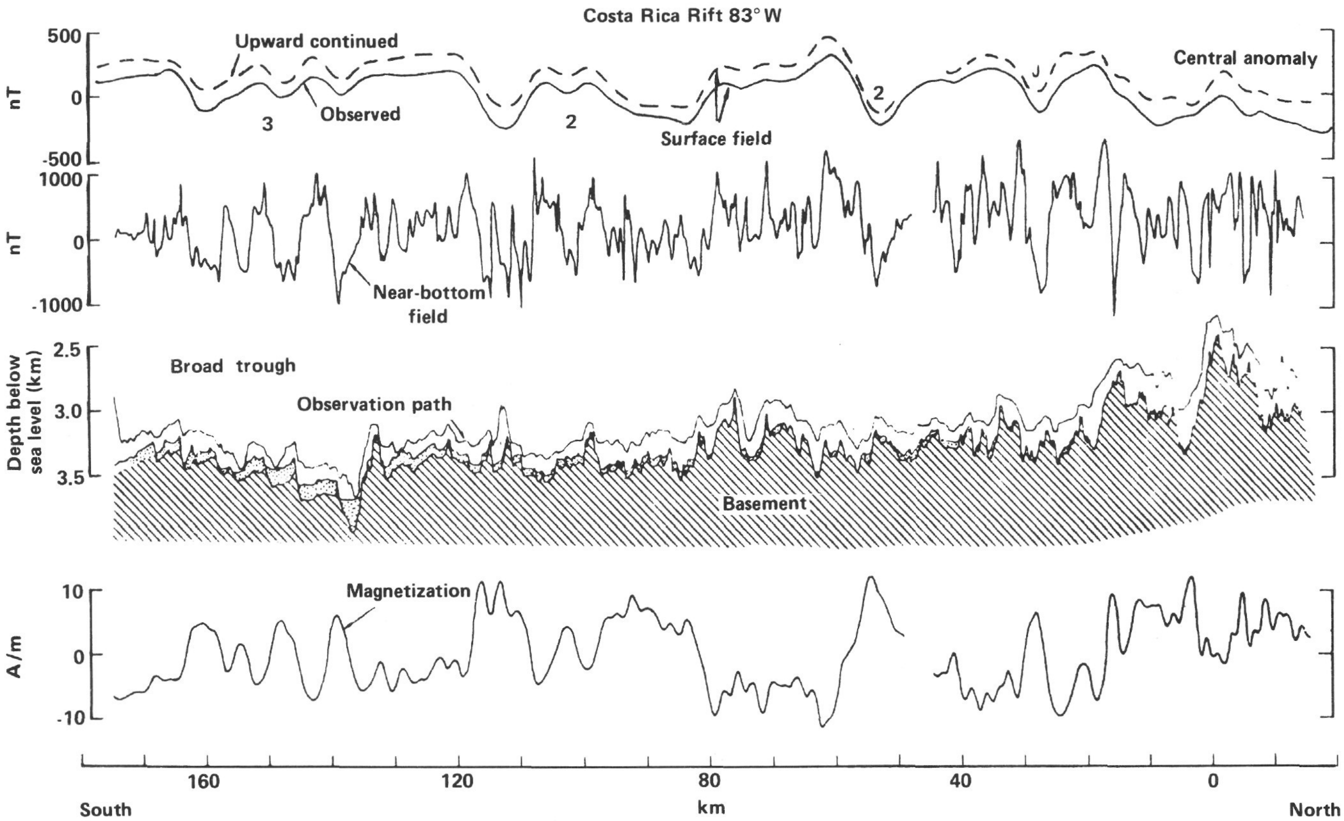

Figure 5. Deep Tow and surface-ship data over the south flank of the Costa Rica Rift from South Tow Leg 6 (Klitgord et al., 1975).

closest area of basement outcrop to Sites 501/504. We will discuss this further below.

HEAT FLOW

Thermal Gradient Measurements

The temperature gradient measurements on *Conrad* 21-17 were taken with two types of instruments. Virtually all of the measurements reported in Table 1 were made with the Digital Heat Flow instrument. This is a modified version of an instrument originally developed by R. Von Herzen of the Woods Hole Oceanographic Institution. The thermistor probes are mounted on outriggers several cm away from a solid lance that is attached to a corehead weight. This is used to obtain multiple bottom penetrations during one lowering from the surface (one "pogo" station). The instrument is dropped into the bottom and is left there for several minutes. This permits one to correct for the effects of transient frictional heating which occurs when the lance is dropped into the bottom. The instrument also monitors bottom-water temperature and the tilt of the instrument package. After a measurement has been obtained, the probe is pulled out of the bottom and the ship then steams at 1–2 knots to the next measurement location. The corehead is not hauled up to the surface but is instead permitted to trail behind the ship as it moves. We then stop at the next point where a measurement is desired, wait for the wire to straighten out, so that we have a vertical angle of penetration, and make the next measurement.

Two piston core measurements were made with a thermograd instrument (Gerard et al., 1962). Subsequently we have routinely used the Digital Heat Flow unit for piston cores, but on *Conrad* 21-17 we had only one DHF unit aboard and the thermograds permitted us to continue operation while recharging the batteries of the DHF.

The heat flow measurements are presented in Table 1. These results, along with four values from Cocotow 4 (Anderson and Hobart, 1976) and five values from DSDP Sites 501, 504, and 505, are shown in Figure 9.

Thermal-Conductivity Measurements

Thermal conductivities were measured on the two piston cores. The needle-probe method was used (Von Herzen and Maxwell, 1959) and the values were corrected to *in situ* conditions (Ratcliffe, 1960). The results are shown in Figure 10. The conductivity varies very little in the rather uniform upper layers of the sediment. The results agree with the uppermost DSDP shipboard measurements from Sites 501/504 and 505 (Wilkens and Langseth, 1983).

RESULTS

There are two main observations that can be made about the heat-flow results in our survey area: (1) In the northern part of the area, near Site 505, the heat flow is low and highly variable. (2) Near Sites 501/504 in the south the heat flow is much higher and much more uniform (in relation to its magnitude).

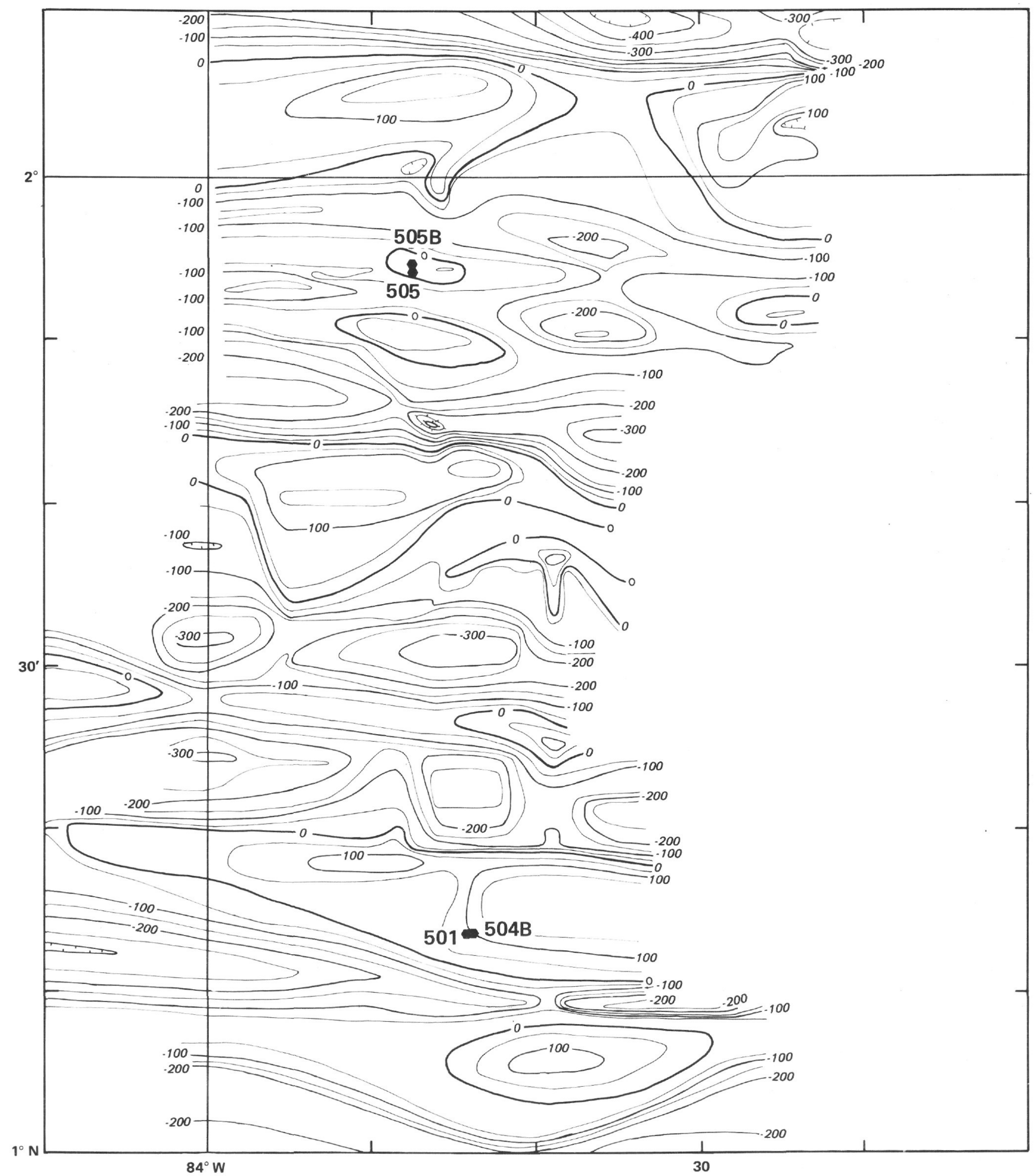

Figure 6. Magnetic anomaly contours in detailed survey area from *Conrad* 21-17 data, 50 nT contours interval.

Our heat-flow survey consists mainly of two lines of stations. A long line of "pogo" stations runs north-south for about 100 km from north of Site 505 to south of Sites 501/504. A cross line runs east-west just south of Sites 501/504 (Fig. 9). We have taken the heat-flow data and projected then onto a north-south seismic profiler line in Figure 11. The dramatic change in character of the heat-flow pattern from scattered values far below the predictions from plate cooling models (Sclater and Francheteau, 1970), to fairly tightly grouped values dis-

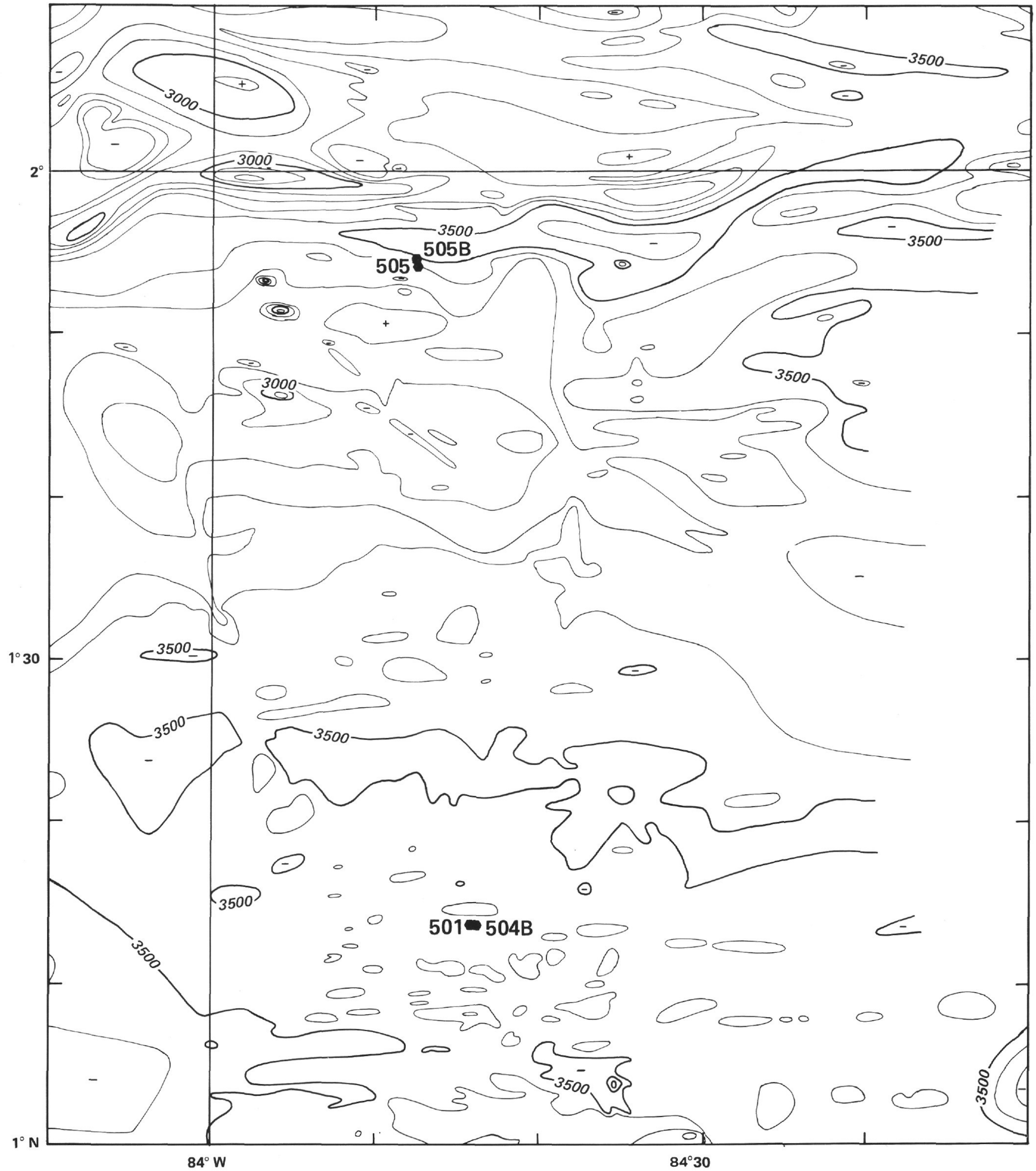

Figure 7. Bathymetric map of detailed survey area, 100-m contour interval.

tributed about the theoretical, is clearly seen. The thickening of the sediment cover to the south is also readily apparent.

The thick sediment cover in the south and the lack of basement outcrops (discussed in more detail later) prevent any hydrothermal systems within the basement from communicating with the ocean. The result is that in the south the measured conductive heat flow is in agreement with the theoretical predictions. The northern area, by way of contrast, with its many fault scarp exposures of basement, offers many areas for circulating seawater to transport heat from the crust to the ocean. The conductive heat flux is therefore far below theoretical. The amount of exposed seafloor does not have to be large in

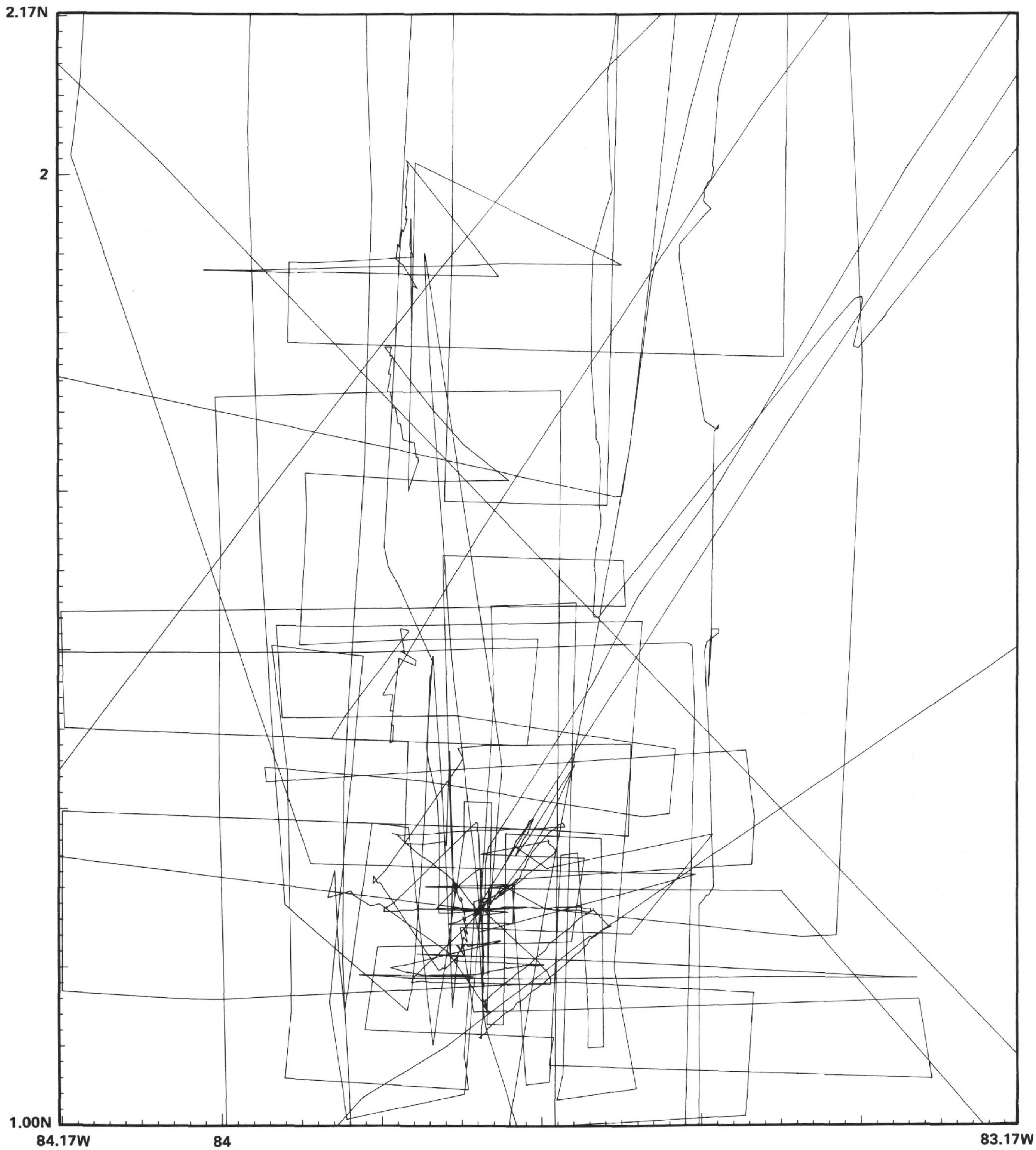

Figure 8. Ship tracks used to construct Figure 7.

area to have a large effect on the heat flow, as the last few outcrops in the north occur near DHF 18A, which still has a low heat flow. We had one attempted measurement between DHF 18A and 18B; it bounced off an outcrop area which, we believe, is the southernmost one along our line of measurements.

It is worth pointing out that none of our measurements exhibited nonlinear temperature profiles. Nonlinearity can indicate water advection through the sediment and has been observed in other areas on the flanks of ridges (Anderson et al., 1979). Fluid flow through sediments occurs when the combination of sediment thick-

Table 1. *Conrad* 21-17 heat-flow stations.

Station	N Latitude	W Longitude	Depth (m)	N_p	Gradient (°C/km)	Thermal conductivity (W/m-K)	Heat flow (mW/m^2)
DHF 14A	1°10.0′	83°46.1′	3461	5	313	(0.716)	224
B	1°10.8′	83°44.9′	3407	6	294 ±38		210 ±27
C	1°11.2′	83°45.1′	3395	6	355		254
D	1°11.8′	83°44.8′	3446	5	258		185
E	1°12.2′	83°44.8′	3463	6	216		155
F	1°13.0′	83°45.0′	3480	5	304 ±40		218 ±29
G	1°13.0′	83°45.0′	3472	5	301 ±39		216 ±28
H	1°14.2′	83°45.1′	3422	6	253		181
I	1°15.1′	83°45.3′	3425	6	274		196
DHF 15A	1°24.1′	83°45.7′	3540	6	227		162
B	1°22.8′	83°45.6′	3531	6	270 ±35		193 ±25
C	1°21.8′	83°45.7′	3497	6	259		185
D	1°21.0′	83°45.4′	3489	6	266 ±34		190 ±24
E	1°19.6′	83°45.4′	3456	6	254		182
F	1°19.1′	83°45.6′	3429	6	250		179
G	1°17.3′	83°45.6′	3433	5	419 ±54		300 ±39
H	1°16.1′	83°45.4′	3459	6	261		187
I	1°15.1′	83°45.2′	3440	6	268		192
DHF 16A	1°10.4′	83°39.8′	3384	6	251		180
B	1°10.2′	83°41.2′	3407	6	243		174
C	1°10.0′	83°42.4′	3425	6	276 ±36		198 ±26
D	1°09.8′	83°43.3′	3437	6	240		172
E	1°09.6′	83°44.3′	3456	6	272 ±35		195 ±25
F	1°09.6′	83°44.7′	3459	6	244		175
G	1°09.6′	83°45.6′	3463	6	270		193
H	1°09.6′	83°46.0′	3459	6	308 ±40		220 ±29
I	1°09.6′	83°47.0′	3459	6	330 ±43		236 ±31
J	1°09.7′	83°48.4′	3455	5	315 ±41		226 ±29
K	1°09.8′	83°49.6′	3463	5	321 ±42		230 ±30
DHF 17A	1°56.9′	83°48.2′	3361	6	20		14
B	1°50.2′	83°48.1′	3179	6	141		101
C	1°51.8′	83°48.1′	3299	4	68		50
D	1°52.9′	83°47.8′	3376	6	92 ±12		66 ±9
E	1°54.7′	83°49.1′	3356	6	123		88
F	1°55.5′	83°48.9′	3504	6	49		35
G	1°56.2′	83°48.8′	3527	6	13		9
H	1°56.5′	83°48.7′	3450	6	16		11
I	1°57.2′	83°48.5′	3370	6	32		23 ±3
J	1°57.9′	83°48.5′	3356	6	38		27 ±4
K	1°58.6′	83°48.5′	3122	6	77		55
L	1°59.8′	83°48.3′	3277	5	151		108
DHF 18A	1°40.6′	83°47.7′	3158	5	84 ±11		60 ±8
(bounce)	1°42.0′	83°47.7′	3150				
B	1°42.1′	83°47.8′	3101	5	134		96
C	1°43.1′	83°48.3′	3135	5	70		50
D	1°44.2′	83°48.9′	3197	5	112 ±15		80 ±11
E	1°45.1′	83°49.3′	3158	5	102 ±13		73 ±9
F	1°46.3′	83°49.6′	3211	5	91		65
G	1°47.6′	83°49.6′	3235	5	116 ±15		83 ±11
H	1°47.8′	83°49.6′	3211	6	33		24
I	1°49.4′	83°49.7′	3233	6	106		76
DHF 19A	1°31.4′	83°48.7′	3375	5	185		133
B	1°30.0′	83°48.7′	3390	5	252 ±33		180 ±24
C	1°29.3′	83°48.2′	3358	5	248 ±32		178 ±23
D	1°24.2′	83°49.4′	3520	5	223		160
E	1°25.2′	83°49.4′	3489	5	224		160
F	1°25.9′	83°49.6′	3450	5	252 ±33		180 ±24
G	1°26.7′	83°49.9′	3388	5	248 ±32		178 ±23
TG6	1°11.5′	83°44.8′	3375	5	270	0.741	200 N_k 53
TG7	1°55.5′	83°48.2′	3504	5	42	0.714	30 N_k 43

Note: N_p = No. of temperature-depth points per station, N_k = no. of thermal conductivity measurements per core.

ness and permeability makes that route either the path of least hydraulic resistance or a negligible barrier. Most of our survey area, however, either has great thicknesses of sediment or nearby bare rock outcrops which would provide much easier locations for fluid outflow.

We have plotted the observed heat flow values in Figure 11 against the theoretical values for the cooling plate (Fig. 12). This presentation, after Hobart et al. (in press), is useful in showing how important the venting of convective heat transfer is in suppressing the conductive heat flow. We should also point out that the heat flow measurements at Sites 501, 504, and 505, which are also shown, are in close agreement with our surface measurements and well within the range of local variability.

The ratio of heat flow to theoretical heat flow, Q/Q_{th}, in the northern area is roughly constant at 0.3. The values of Q/Q_{th} in the south seems to show an increase with age. This value increases from 0.84 at 5.31 Ma to 1.04 at 5.84 Ma and 1.05 at 6.02 Ma. The latter two values are indistinguishable given the nearly uniform sample groupings of about a dozen used for the averages. This increase in the averages, and especially the trend visible in Figure 12, suggests to us that some type of thermal recovery phenomenon is taking place in the conductive heat flow.

CONDUCTIVE RECOVERY MODEL

Once the basement exposures in the north are covered with sediment, then the increase in heat flow as one moves south into older crust represents either the time that it takes for the crustal layer cooled by convection to reheat or the lateral distance that a convective system can "steal" heat.

We have modeled the conductive recovery hypothesis in a fairly simple way. The model has the following assumptions:

1. There are two layers in the crust, both having the same physical properties. The first layer is from $0<x<L$ and the second layer continues for $x>L$, where x is in the vertical direction and L is the thickness of the layer.
2. The surface temperature T at $x = 0$ is held constant at $T = 0$ for all times, t.
3. The heat flux coming from the lower layer to the upper layer at $x = L$ is held constant at F_o.
4. The upper layer is held at temperature $T = 0$ until time $t = 0$ and is then allowed to heat conductively from below because of flux F_o.

The solution to this model is given by Carslaw and Jaeger (1959, section 3.8, equation 6); we reproduce it below:

$$V = \frac{2(\kappa t)^{1/2}}{K} \sum_{n=0}^{\inf} (-1)^n \left\{ \mathrm{ierfc}\, \frac{(2n+1)L-x}{2(\kappa t)^{1/2}} - \mathrm{ierfc}\, \frac{(2n+1)L+x}{2(\kappa t)^{1/2}} \right\} \qquad (1)$$

We then differentiate Equation 1 with respect to x and obtain the following:

$$\frac{dV}{dx} = \frac{-F_o}{K} \sum_{n=0}^{\inf} (-1)^n \left\{ \mathrm{erfc}\, \frac{(2n+1)L-x}{2(\kappa t)^{1/2}} - \mathrm{erfc}\, \frac{(2n+1)L+x}{2(\kappa t)^{1/2}} \right\} \qquad (2)$$

The surface heat flow is given by Equation 2 evaluated at $x = 0$, which simplifies to just:

$$F_{x=0} = K \frac{dV}{dX_{x=0}} = -2F_o \sum_{n=0}^{\infty} (1-1)^n \, \mathrm{erfc}\, \frac{(2n+1)L}{2(\kappa t)^{1/2}} \qquad (3)$$

We have plotted the surface heat flow as a fraction of the heat flow from the lower layer, F_o, using Equation 3, in Figure 13A. This shows the result of the calculation using various layer thicknesses; it has been calculated using the available physical property data from Hole 504B (Karato et al., 1983; Karato, 1983).

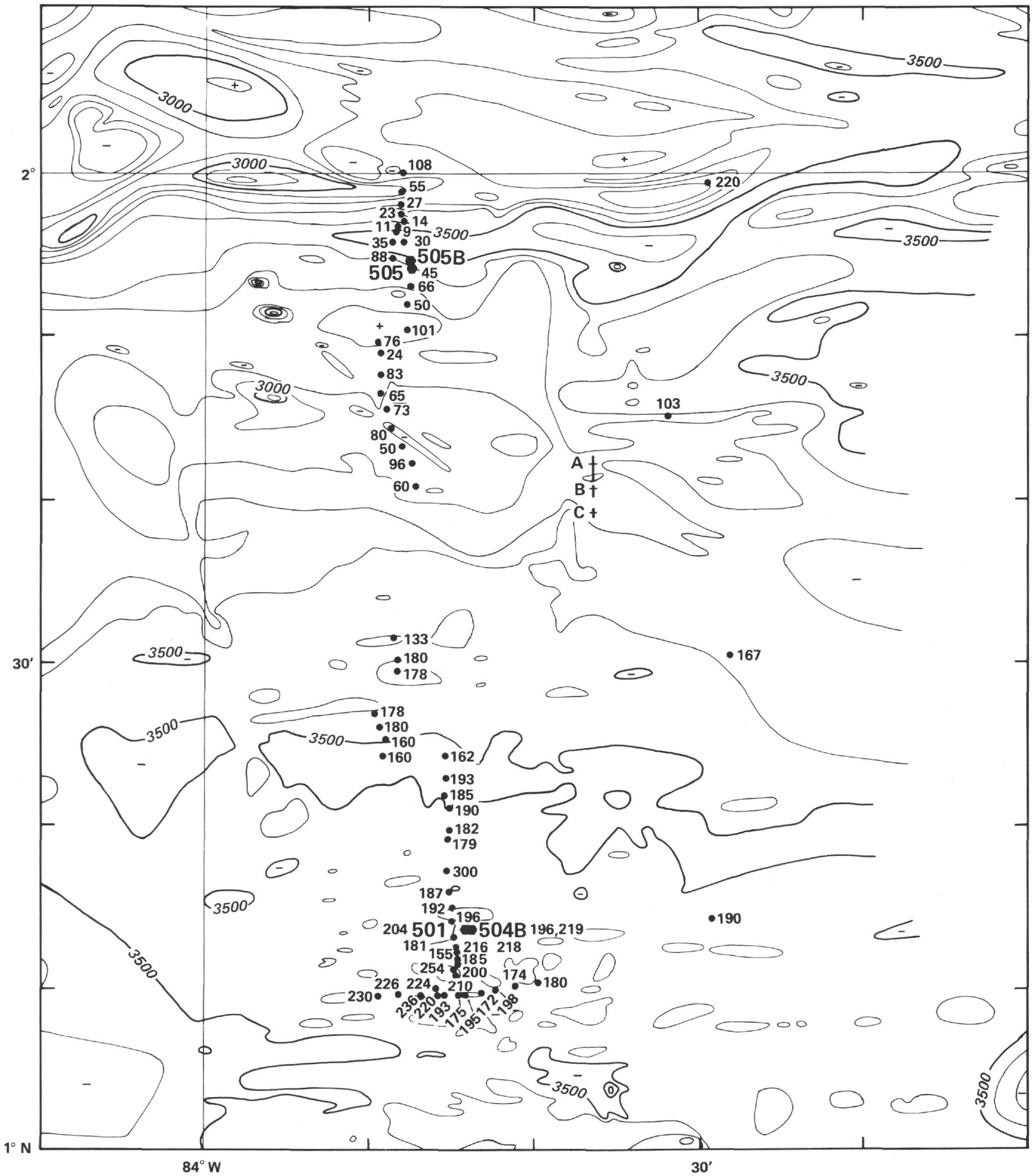

Figure 9. Heat-flow measurements in detailed survey area. Values are in mW/m^2 (1 mW/m^2 = 0.02389 μcal/cm$^2 \cdot$s). A, B, C represent locations of South Tow 6 Deep Tow tracks.

We may now compare this simple conductive reheating model to the data which we presented in Figure 12. Two important caveats are (1) The heat flow before the reheating was not zero, but was about 0.3 of what it should have been. Therefore, the temperatures within the upper layer were not zero. (2) We believe that this existing heat flow was due to hydrothermal circulation. This circulation may not turn off completely during the recovery process, and would therefore act to increase the effective thermal diffusivity of the upper layer. The recovery that we observe would therefore be quicker than otherwise expected for a layer of a given thickness and

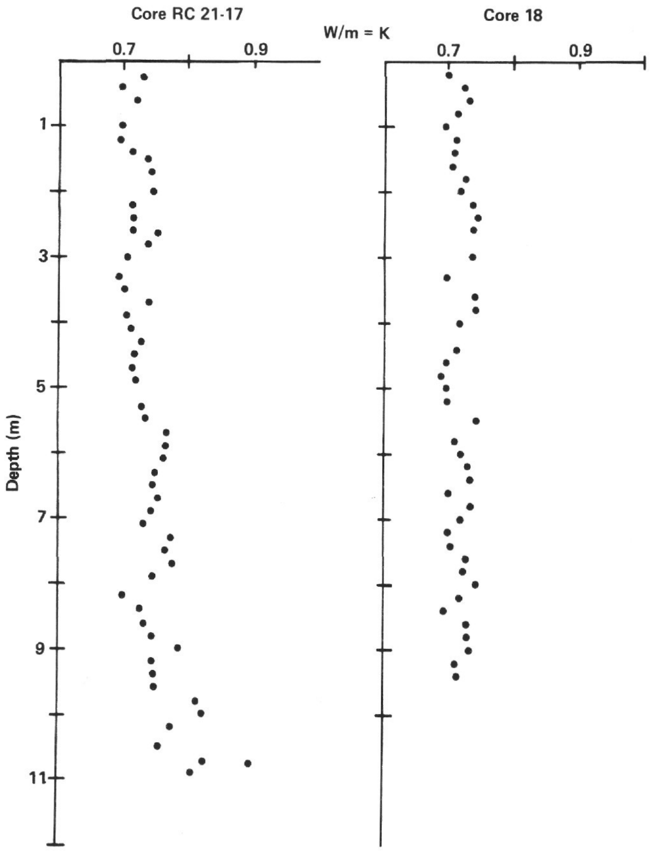

Figure 10. Thermal conductivity versus depth below seafloor for cores *RC*21-17 (TG6) and *RC*21-18 (TG7), *Conrad* 21, Leg 17. Values in W/m-K (1 W/m-K = 2.389 mcal/cm·-s °C).

would represent a thicker layer, given a certain specified recovery time.

We observe in Figure 12 that the recovery has started somewhere in the time between 4.5 and 5.0 Ma (the usual data gap caused by cruise scheduling problems; it will be filled in on a forthcoming cruise). The recovery continues until at least 5.8 Ma. It is difficult precisely to scale the existing data to fit onto Figure 13A, but when one makes the attempt, the data fall along the 5- to 6-km-layer curves (Figure 13B). It is clear that the layer must be near this thickness as the thinner layers do not permit the model to fit the slow increase in heat flow that is observed over 5- to 5.8-Ma crust. The recovery must therefore begin shortly after the last area of exposed crust is covered, near crust of 4.5-Ma age.

An alternative to the conductive recovery model is that the heat is being transported laterally by hydrothermal cells "mining" the heat out from under a sedimentary cover that is thick and impermeable. This type of phenomenon is rather difficult to model and will limit our comments to the observation that the heat flow is still increasing with age to distances much farther than the distance from the nearest outcrop to Sites 501/504 in the south. We will discuss this inconsistency further in the next section along with the distribution of basement exposures.

The observation by Becker et al. (1983) that the lower several hundred meters of Hole 504B were not subject to convective flow and the projected agreement with the sediment temperatures lend considerable support to the conductive recovery model. Even though the basement was permeable enough to support convection (Anderson and Zoback, 1982), the flow rates were either negligible or slow enough that our model may well be reasonable.

BASEMENT OUTCROPS AND THEIR ROLE IN CONTROLLING HEAT FLOW

We have considerable information about the distribution of sediment cover and the location of basement outcrops within our survey area. Surveys of this area have been carried out with the GLORIA long-range side-scan sonar system (Searle, 1983) and the Deep Tow near-bottom side-scan sonar system (Klitgord et al., 1975). These complement the 3.5-kHz and 12-kHz echo sounders and single-channel seismic systems of the ship.

A summary of the GLORIA survey results is presented in Figure 14 (Searle, 1983). Searle's work shows that in the northern part of our survey area, near Site 505, about 17% of the seafloor consists of basalt outcrops.

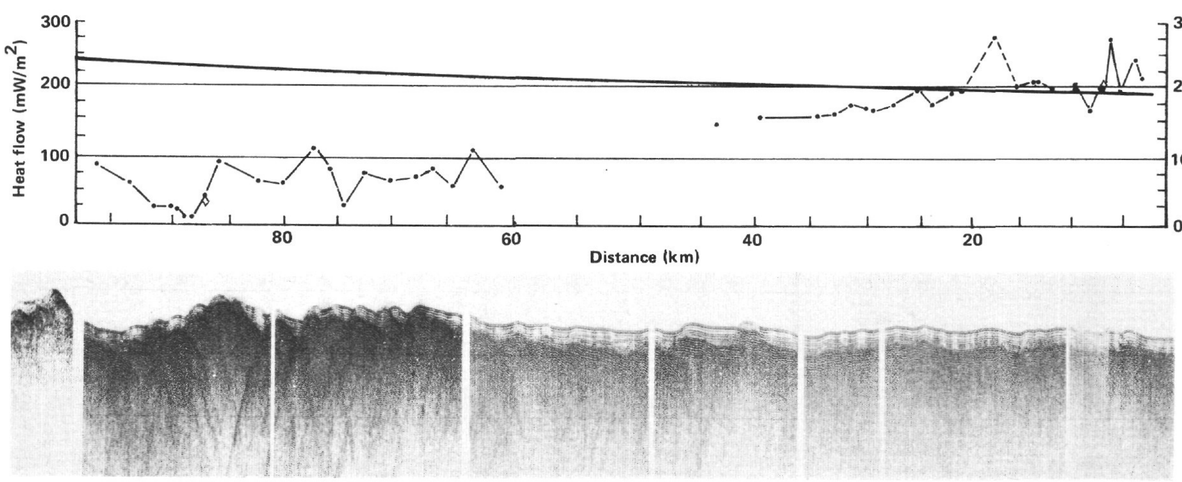

Figure 11. Heat flow measurements projected onto *RC*21-17 north–south seismic profiler line.

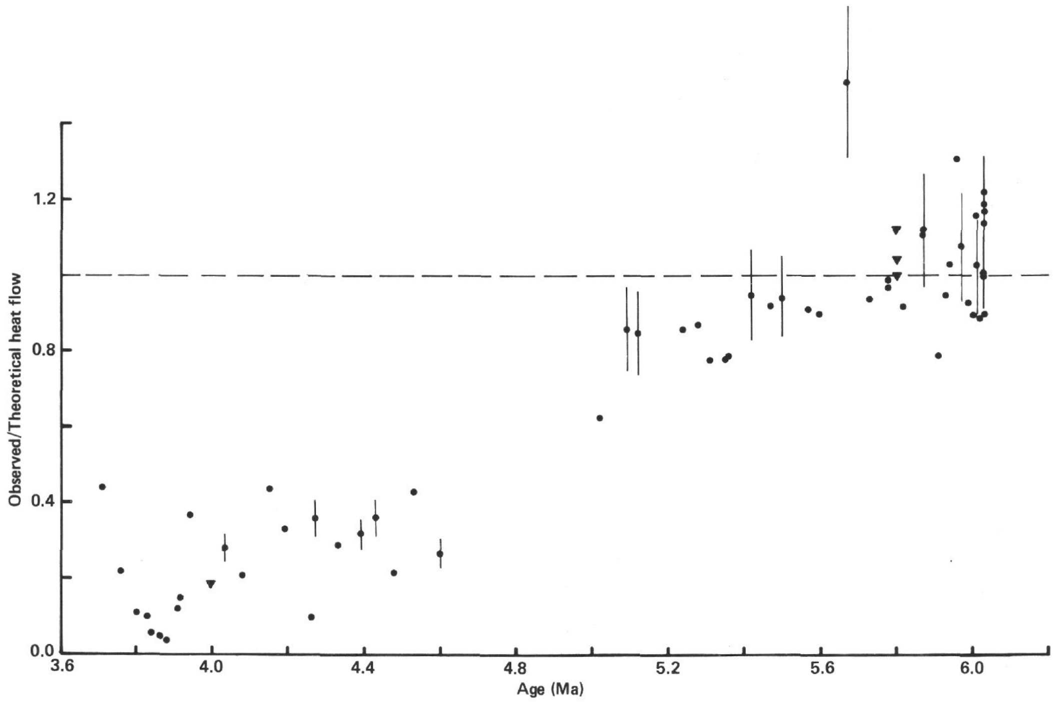

Figure 12. Heat flow profile normalized by theoretically predicted values from a plate cooling model (Sclater and Francheteau, 1970). Bars show limits on measurements where instrument tilted; most values are probably near the lower limit (i.e., a lower correction than postulated).

His figure shows the outstanding linearity and continuity of the fault scarps and lines of outcrop along the northern trough. The fault scarps all face to the north, toward the spreading center. The northern wall of the trough has linear basalt outcrops, but does not have inward-facing fault scarps. It is not a graben structure.

The southern area, near Sites 501/504, has lines of buried fault scarps but very little exposed basement. Searle shows several small areas of basement exposures just south and southwest of Sites 501/504. We believe, after re-examining the available echo-sounding and seismic profiler records, that there is no basement exposure in this vicinity. These areas are close to the *Discovery*'s track and we believe that they are areas of stronger reflection from unusually smooth seafloor. Figure 15 shows 3.5-kHz and seismic-profiler records over this area of disputed outcrops. Figure 16 shows the seismic-profiler records over Sites 501/504 and Site 505.

In contrast, there is no dispute that the fault scarp and basement exposures we had found near 1°00′N, 83°30′W on *Conrad* 21-17 are correct. They stand out strongly on the GLORIA records.

The Deep Tow profile from South Tow Leg 6 has been discussed previously (Fig. 5). We have examined the original Deep Tow records to study the nature of the basement exposures and sediment blanket in the northern part of our survey area. Figure 17 shows several near-bottom bathymetric and 4-kHz echo-sounding profiles of the southernmost areas of outcropping basement along the Deep Tow line. The location of these profiles is shown in Figure 9 (A, B, and C). Figure 17A is a typical scarp for the northern part of the survey area. The scarps along the south wall of the major east-west trough are very similar but are found closer together and the sediment cover is somewhat less. The change in slope from the scarp itself to the talus pile beneath it is easily seen. The near-surface ash layer (layer "L" of Bowles *et al.*, 1973; Ninkovich and Shackleton, 1975) is shown also. It can clearly be seen to pinch out as the base of the scarp is approached, indicating a decreasing sedimentation rate caused by bottom-current activity. The bottom currents in this region are not well known, but this observation is in accord with what is known of the bottom circulation in the Panama Basin (Laird, 1969, 1971; Kowsman, 1973; Lonsdale, 1977b).

Figures 17B and 17C show the southernmost outcrop and the southernmost detection of basement seen by the Deep Tow instrument. The outcrop in Figure 17B is very small, but the heat-flow evidence cited above implies that it may still play an important role in venting the basement. A similarly small outcrop to the west was found as we bounced our heat-flow probe off it. The basement structure in Figure 17C is more irregular in nature and may have some constructional components in it, similar to those seen on the Galapagos Spreading Center (Lonsdale, 1977a). An area of thin sediment cover such as this might be a locus of fluid flow through the sediments (Anderson et al., 1979), although we did not happen to detect any such areas in our geothermal survey.

The left- and right-looking side-scan sonar records accompanying Figure 17A are shown in Figure 18. Areas of basalt outcrop are dark black because of the high acoustic return. Note that the basement structure shown near 2.2 km in Figure 17A does outcrop slightly to the west of the fish track, as shown by the left-looking sonar.

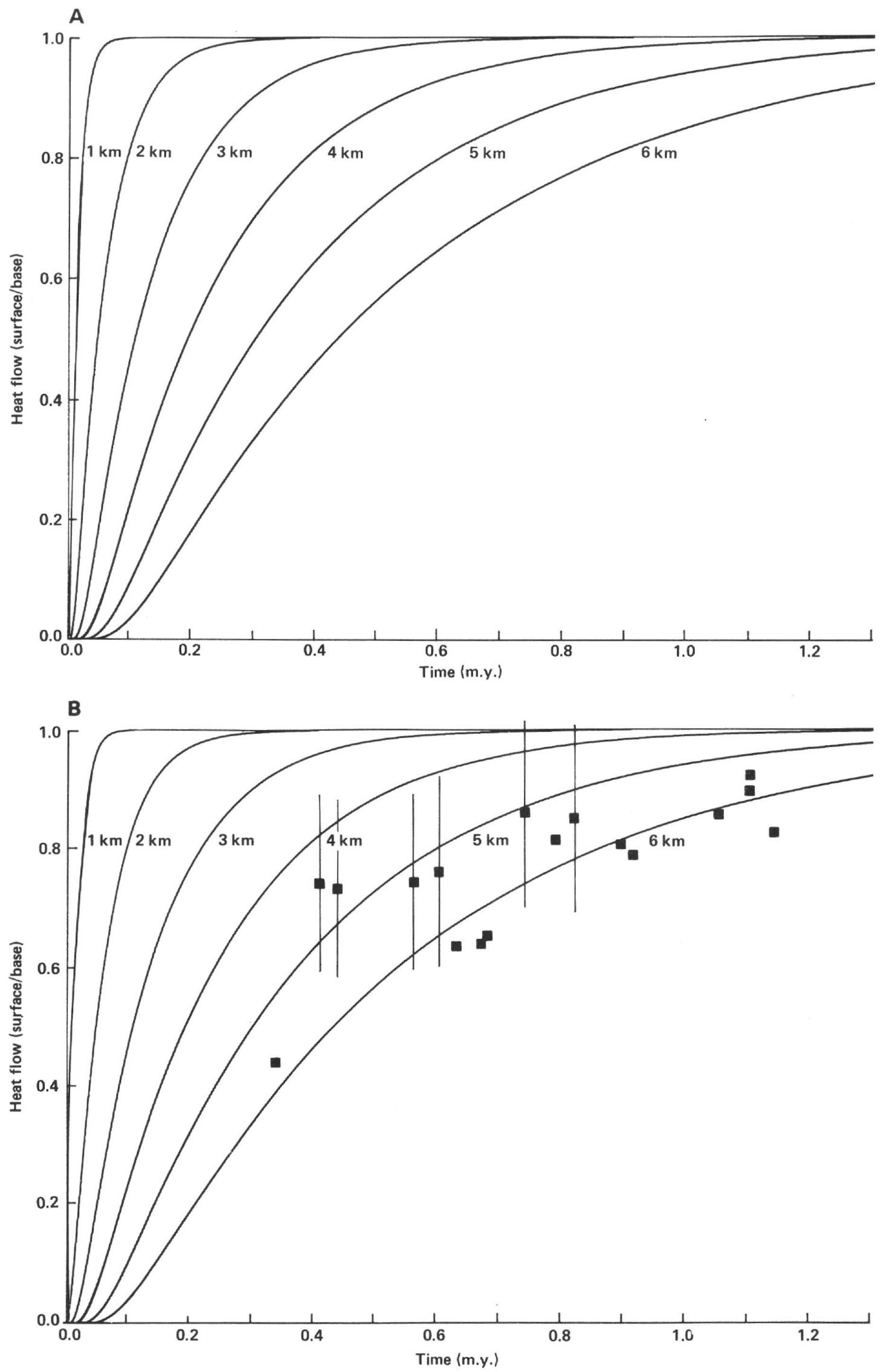

Figure 13. A. Results of conductive recovery model (Equation 3) for various thicknesses of the layer that is cooled (in km). B. Heat flow data from Figure 12, scaled and projected onto Figure 13A. See text for cautions in interpretation.

We have compiled a sediment isopach map for our survey area (Fig. 19). The map shows the general pattern of sedimentation that we have discussed earlier: thin and irregular sediment cover in the northern part of the survey area and thick and uniform cover in the southern part. Certain small areas where the sediment thins in the southern area do stand out. These are also areas of basement outcrops found by the GLORIA survey (Fig. 14).

CRUSTAL STRUCTURE

The structure of the upper levels of the crust on the south flank of the Costa Rica Rift was studied on *Conrad* 21-17 by an intense sonobuoy refraction program.

The data were obtained using the *Conrad*'s large-volume air gun system as a sound source and U.S. Navy sonobuoys as receivers. Three sonobuoys were success-

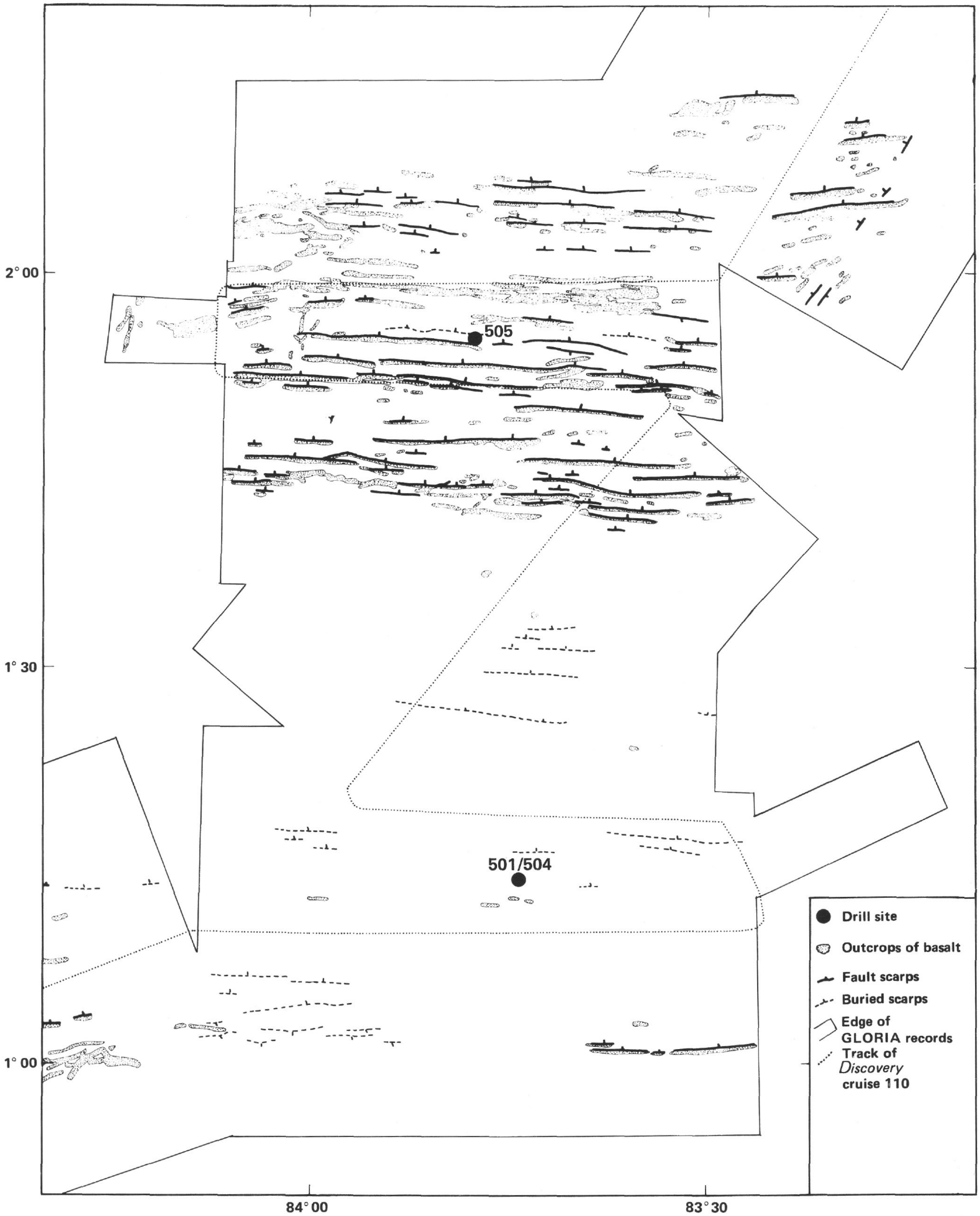

Figure 14. Interpretation of *Discovery* cruise 110 GLORIA records (Searle, 1983). Possible outcrops near 1°12 N, 84°00 W discussed in text.

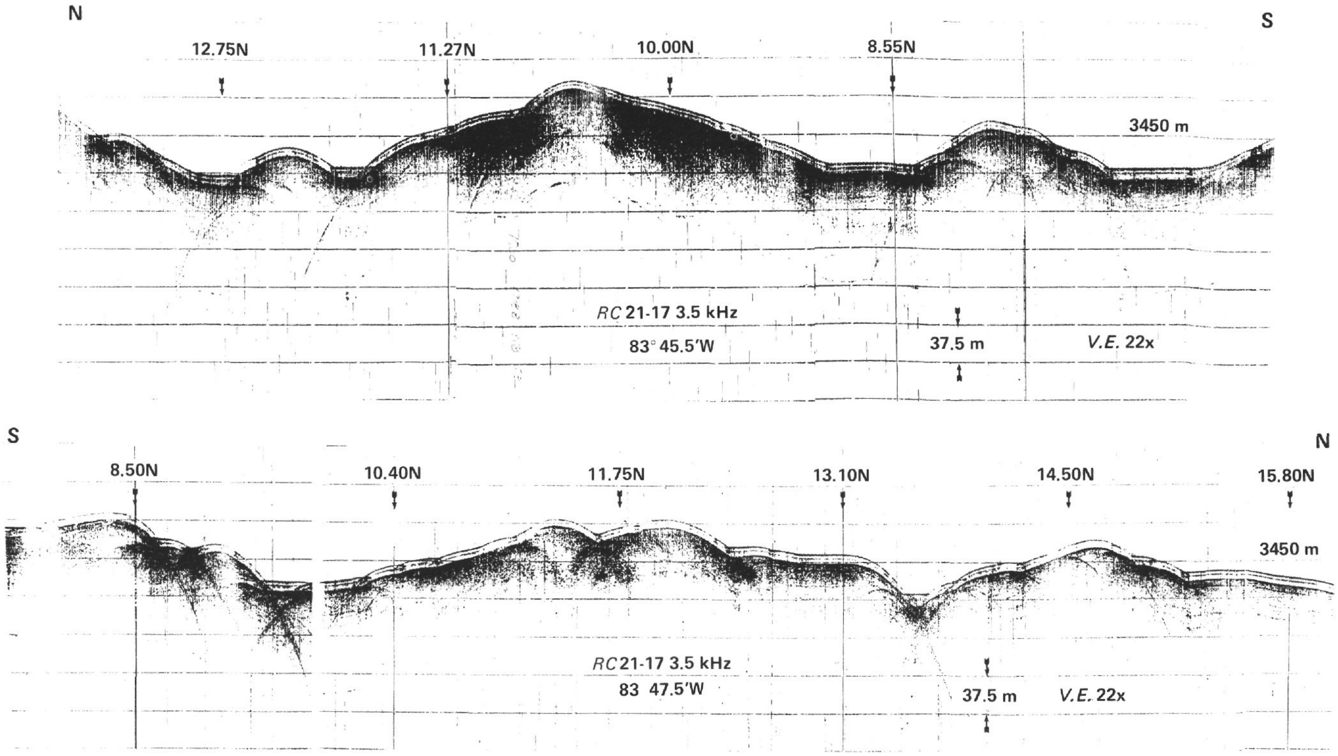

Figure 15. Profiler and 3.5-kHz records over area of possible outcrops, near 1°12 N latitude.

ful on a north–south run from the ridge crest to the survey area. Twelve sonobuoys were run in the survey area shown in Figure 7. One sonobuoy was obtained just south of that area, in the southern extension of our *Conrad* survey. The locations of the sonobuoys are shown in Figure 20 along with the DSDP sites and the locations of the heat-flow measurements.

The results of the sonobuoy runs were excellent, with clear water and refraction arrivals. S-wave conversion arrivals were clearly seen in the sonobuoy records from the southern part of the survey area. The sonobuoy results are presented in Table 2. We present the crustal structures determined from the sonobuoys as conventional "layer-cake" solutions since we only recorded the data in an analog manner and the sonobuoys transmitted "compressed" data using an automatic gain control (AGC) circuit.

We can conveniently divide the sonobuoys according to whether or not shear wave arrivals were detected. The sonobuoys with shear arrivals were found in the area of high heat flow whereas the sonobuoys without shear arrivals were located in the zone of low heat flow. The compressional-wave solutions in the high-heat-flow zone are shown in Figure 21. In many instances, refractors from the uppermost basement layer were observed as first arrivals. These velocities are thus determined with considerable confidence. They average 4.7 km/s, but range widely from 4.3 to 5.1 km/s. The mean velocity in the uppermost layers is considerably higher than that commonly found in Layer 2A for 5-Ma-age crust (Houtz and Ewing, 1976). The low velocities of Layer 2A are commonly observed in oceanic crust of this age on ridge flanks and are thought to be associated with the highly fractured volcanic carapace.

The shear waves from the lower parts of Layers 2 and 3 were seen for nearly all of the sonobuoy profiles in the southern part of the survey area. The solutions are shown in Figure 22. The variability is much reduced compared to the compressional-wave results, typical of other refraction work. Poisson's ratios were calculated using the V_p/V_s ratio. Values of 0.30 were found over the top 3.5 km; they decreased to about 0.22 below that depth (Fig. 24, later). This decrease has been reported by Christensen and Salisbury (1975) and is believed to be associated with a gabbroic layer at the base of the crust. The velocity structure observed is rather typical of other oceanic results. The results of Bentley et al. (unpublished manuscript) on the north flank of the Costa Rica Rift are similar.

The results in the low-heat-flow zone over younger crust are shown in Figure 23. Twice we observed low velocities in the uppermost refractor (3.3 and 3.9 km/s). These low velocities may be associated with unusually porous layers. This would be in accord with the heat-flow observations which imply a rather vigorous convective circulation in the younger crust. Generally, the sonobuoy profiles in the younger crust did not see so deeply because of the more rapid attenuation of refracted arrivals with distance.

The mean velocity structure, determined by averaging the plane layer solutions, was presented in Figure 24. This profile is similar to that found by the Oblique Seismic Experiment (OSE), both here in Hole 504B (Stephen, 1983) and in older crust at Site 417 (Stephen et al., 1980).

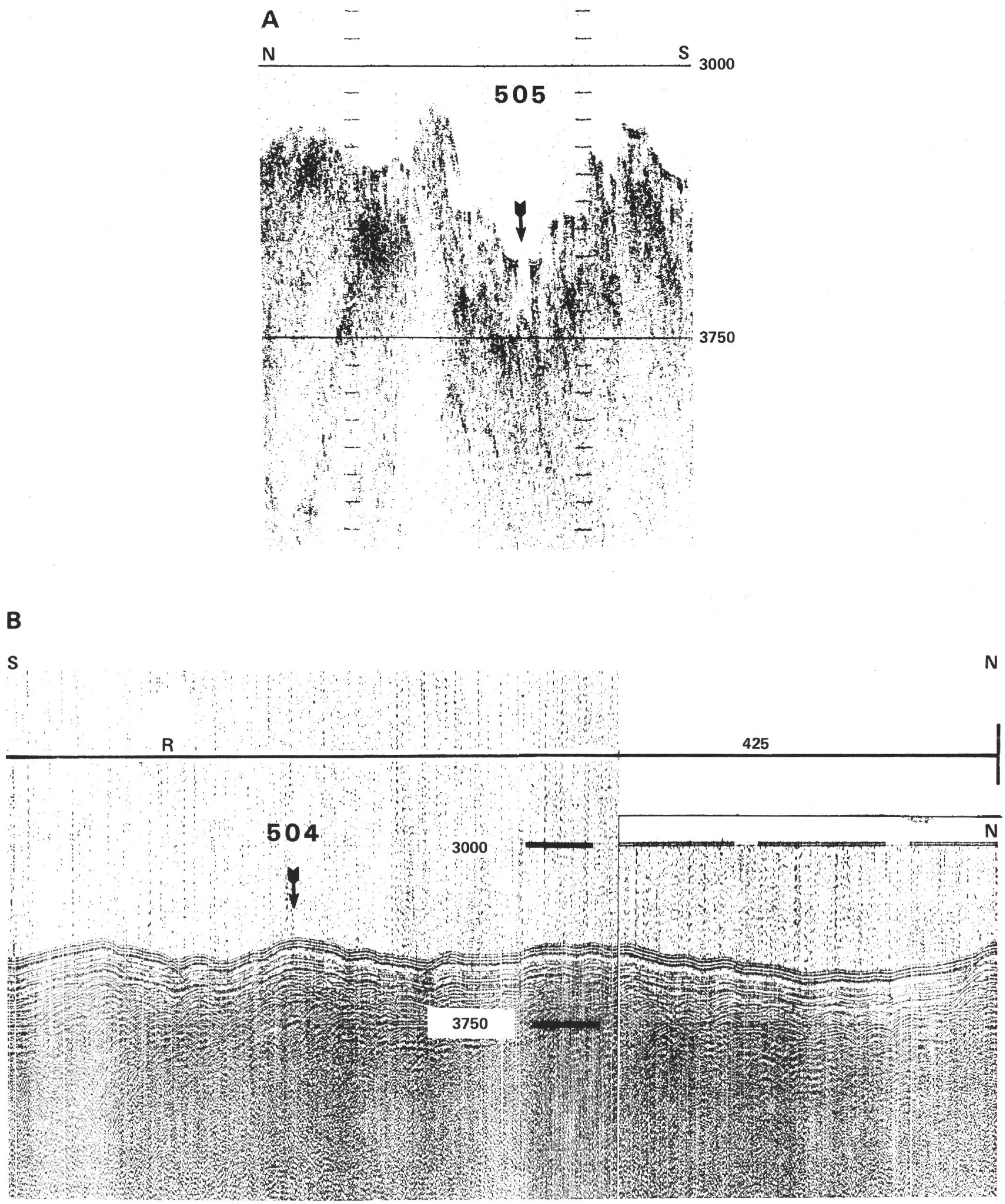

Figure 16. A. Profiler records across Sites 501/504. B. Profiler records across Site 505.

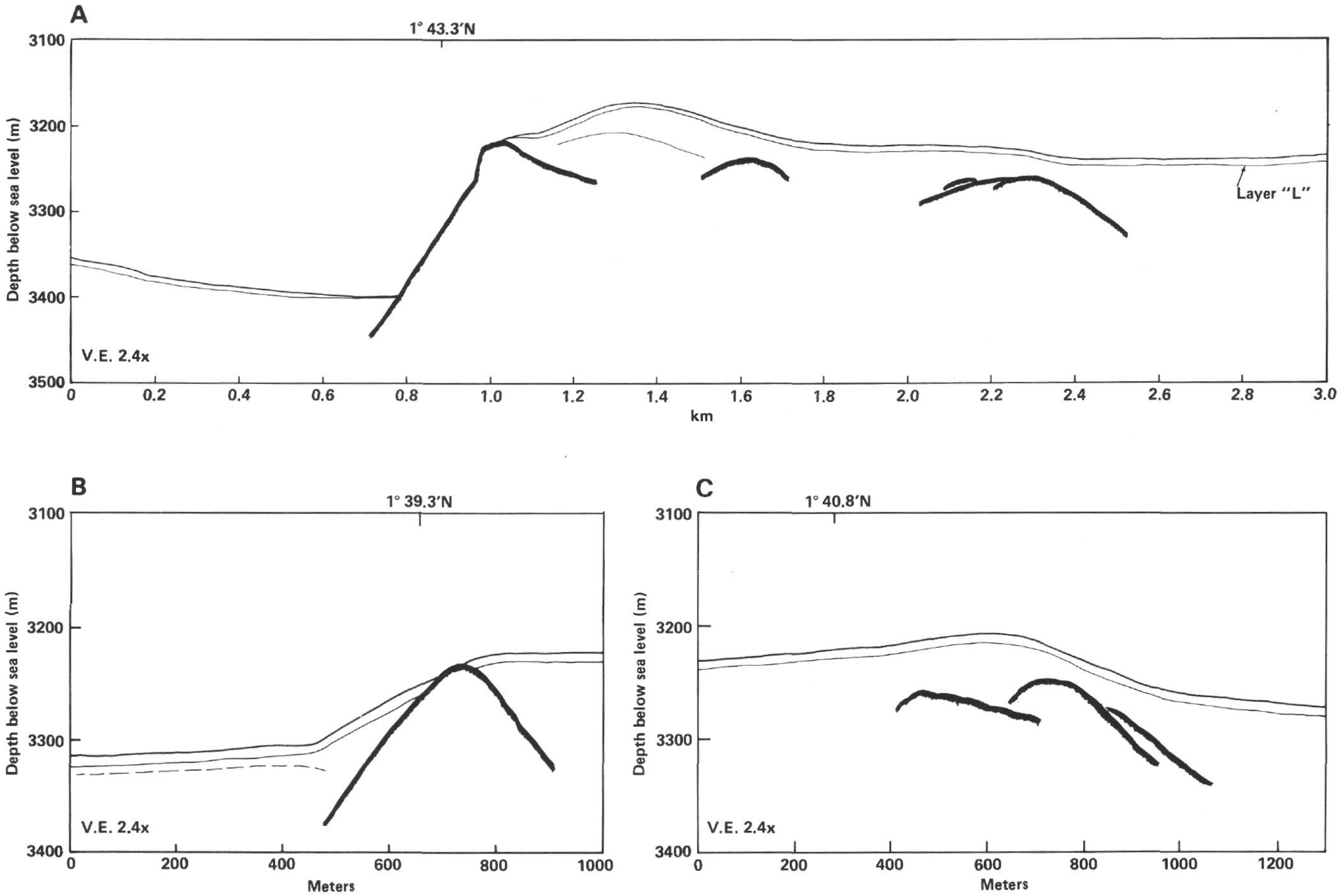

Figure 17. Tracings of South Tow 6 Deep Tow 4 kHz echosounder records (see Fig. 9 for locations). Basement shown as bold shading, ash layers as thin lines. A. Southernmost large scarp (1°42.3′N). Talus pile on scarp causes break in slope. Note pinching of ash layer "L" at base of scarp. B. South of A, southernmost rock outcrop. C. South of B, southernmost record of basement from Deep Tow profile. More complex character of basement may reflect constructional rather than faulting origin.

We have plotted the OSE results and our mean results in Figure 25. The agreement is remarkable, with initial velocities, velocity gradients, and the location of changes in the gradient all quite comparable. This suggests to us that high-quality sonobuoys, if run in a sufficient number, may be used to obtain results similar to the OSE at a considerable savings in cost. We *do not* feel that this technique obviates the need for carrying out Oblique Seismic Experiments; rather, it may fill in for one when there is no deep crustal drill hole available.

GRAVITY

Gravity measurements were obtained on *Conrad* 21-17 using Lamont's Graf-Askania GSS3 gravity meter. The results of the *Conrad* survey are presented in Figure 26 as free-air anomalies. It can be seen that the southern part of the survey area is rather uniform at −10 mgals with only low-amplitude anomalies superimposed on that. The northern part of the area, however, does show anomalies associated with the east-west trough and the ridges on either side of it. The deepest parts of the trough have values as low as −20 mgals while the flanking ridge to the south reaches somewhat above +10 mgals. There is a +20 mgal anomaly in the northwest corner of the survey area which corresponds with a topographic high reaching above 2900 m. However, a narrower ridge reaching even shallower depths just south of this high, and located on the north wall of the east-west trough, does not have a comparable anomaly associated with it.

SEISMICITY

The south flank of the Costa Rica Rift has a small amount of teleseismically determined earthquake activity. The focal mechanism of one earthquake has been determined (Molnar and Sykes, 1969). The epicenter location was just north of our east-west trough. The difference is smaller than the error in the epicenter location. Molnar and Sykes chose to interpret their solution as resulting from motion along a north-south fracture zone. The sense of motion was not in accord with that of the fracture zones flanking the Costa Rica Rift. We choose to reinterpret this focal plane solution as east-west motion along the topographic trough. This may well represent deformation of the south flank of the Costa Rica Rift in response to continued readjustment of the Cocos-Nazca-American plate system. There seems to be some concentration of seismic activity along this east-west topographic trough but further study with a net of ocean bottom seismographs is necessary in order to confirm any activity.

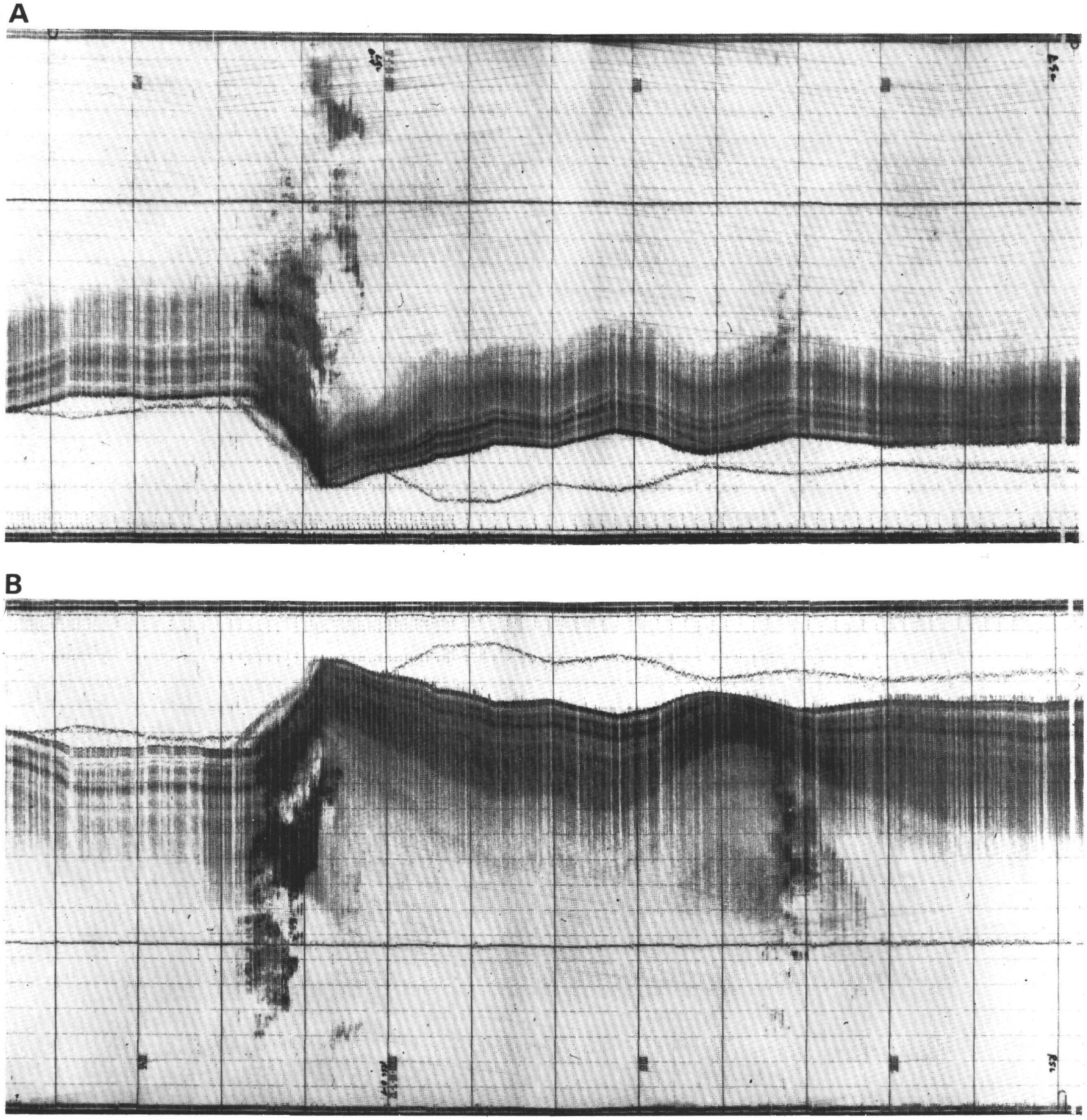

Figure 18. Left- and right-looking Deep Tow side-scan sonar records (A and B, respectively) for Figure 17A. Exposed rocks are dark, showing high reflectivity. (Not corrected for variations in Deep Tow fish altitude above bottom.)

The east–west trough may also represent the site of a future ridge jump to the south of the present spreading axis of the Costa Rica Rift. It is intriguing to note that this trough lines up reasonably well with the crest of the Ecuador Rift segment of the Galapagos Spreading Center just to the west. This must remain simply a speculation for the present.

CONCLUSIONS

The conclusions that can be drawn from this survey relate mainly to the nature of geothermal phenomena in the oceanic crust. It is clear that the role of the sediment cover in blanketing basement exposures plays a crucial role in sealing off convective interchange between the crust and the ocean. On the south flank of the Costa Rica Rift, it appears that the crust, once it is sealed off from the ocean, behaves as if it were a 5–6-km-thick layer conductively reheating from below. The upper layers of the crust within this area of reheating show higher seismic compressional-wave and shear-wave velocities than the area to the north. They also show much less attenuation of these waves, particularly the shear waves.

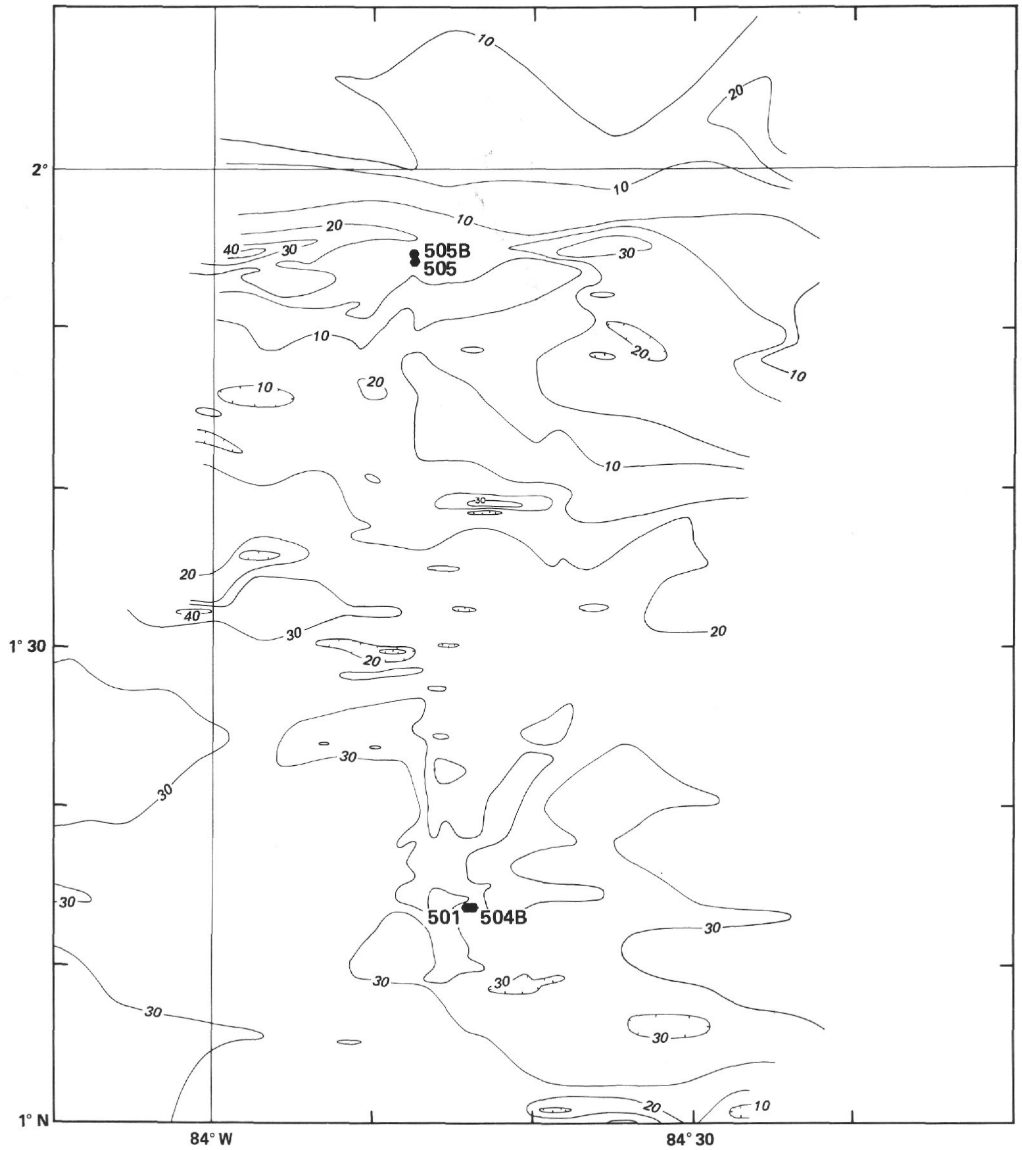

Figure 19. Sediment isopach map of detailed survey area.

This may be due to the sealing of cracks and pores within the upper crust as the temperature and chemistry of the pore fluids change once they have been sealed off from the ocean by the sediment.

In the northern part of our survey area, a major east-west topographic trough within which Site 505 was drilled may well be the site of continuing deformation within the crust of the Nazca Plate. A certain amount of teleseismic activity occurs along the trough, and a strike-slip focal mechanism has been determined for an earthquake along it.

ACKNOWLEDGMENTS

We would like to thank various people for providing copies of their data and for preprints: Ralph Stephen (*Gilliss* 79-04), Roger Searle (*Discovery* 110, "GLORIA"), Peter Lonsdale (South Tow 6, Deep Tow), and George Shor (seismic data). Their comments have also been very useful, as have discussions with Mike Mottl, Keir Becker, and Dick Von Herzen. Captain Jorgensen and the crew of the *Robert D. Conrad* were invaluable. Howard Giddy virtually ran the winch by himself throughout our endless "pogo" stations. Bruce Herman, Dave Roach, and Bill Van Steveninck assisted ably at sea and in the lab. This project was funded by the National Science Foundation through the IPOD Site Survey Program, Grant UC NSF-C482/2 Scope L.

REFERENCES

Allmendinger, R. W., and Riis, F., 1979. The Galapagos Rift at 86°W. 1. Regional morphological and structural analysis. *J. Geophys. Res.*, 84:5379–5389.

Anderson, R. N., Clague, D. A., Klitgord, K. D., Marshall, M., and Nishimori, R. K., 1975. Magnetic and petrologic variations along the Galapagos Spreading Center and their relation to the Galapagos melting anomaly. *Geol. Soc. Am. Bull.*, 86:683–694.

Anderson, R. N., and Hobart, M. A., 1976. The relation between heat flow, sediment thickness, and age in the Eastern Pacific. *J. Geophys. Res.*, 81:1968–1989.

Anderson, R. N., Hobart, M. A., and Langseth, M. G., 1979. Geothermal convection through oceanic crust and sediments in the Indian Ocean. *Science*, 204:828–832.

Anderson, R. N., Langseth, M. G., and Sclater, J. G., 1977. The mechanisms of heat transfer through the floor of the Indian Ocean. *J. Geophys. Res.*, 82:3391–3409.

Anderson, R. N., Moore, G., Schilt, S., Cardwell, R., Trehu, A., and Vacquier, V., 1976. Heat flow near a fossil ridge on the north flank of the Galapagos Spreading Center. *J. Geophys. Res.*, 81: 1828–1838.

Anderson, R. N., and Zoback, M. D., 1982. Permeability, underpressures, and convection in the oceanic crust near the Costa Rica Rift, eastern equatorial Pacific. *J. Geophys. Res.*, 87:2860–2868.

Becker, K., Langseth, M. G., Von Herzen, R. P., and Anderson, R. N., 1983. Deep crustal geothermal measurements, Hole 504B, Costa Rica Rift. *J. Geophys. Res.*, 88:3447–3457.

Bowles, R. A., Jack, R. N., and Carmichael, I. S. E., 1973. Investigations of deep-sea volcanic ash layers from Equatorial Pacific cores. *Geol. Soc. Am. Bull.*, 84:2371–2388.

Carslaw, H. S., and Jaeger, J. C., 1959. *Conduction of Heat in Solids* (2nd ed.); Oxford (Oxford University Press).

Christensen, N. I., and Salisbury, M. H., 1975. Structure and constitution of the lower oceanic crust. *Rev. Geophys. Space Phys.*, 13: 57–86.

Corliss, J. B., Dymond, J., Gordon, L. I., Edmond, J. M., Von Herzen, R. P., Ballard, R. D., Green, K., Williams, D., Bainbridge, A., Crane, K., and van Andel, T. H., 1979. Submarine thermal springs on the Galapagos Rift. *Science*, 203:1073–1083.

Donnelly, T. W., Francheteau, J., Bryan, W., Robinson, P., Flower, M., Salisbury, M., et al., 1980. *Init. Repts. DSDP*, 51, 52, 53: Washington (U.S. Govt. Printing Office).

Gerard, R., Langseth, M. G., and Ewing, M., 1962. Thermal gradient measurements in the water and bottom sediment of the western Atlantic. *J. Geophys. Res.*, 67:785–803.

Hekinian, R., Rosendahl, B. R., et al., 1980. *Init. Repts. DSDP*, 54: Washington (U.S. Govt. Printing Office).

Herman, B. M., Langseth, M. G., and Hobart, M. A., 1977. Heat flow in the oceanic crust bounding western Africa. *Tectonophysics*, 41:61–77.

Hey, R., 1977. Tectonic evolution of the Cocos-Nazca spreading center. *Geol. Soc. Am. Bull.*, 88:1404–1420.

Hey, R., Johnson, G. L., and Lowrie, A., 1977. Recent plate motions in the Galapagos area. *Geol. Soc. Am. Bull.*, 88:1385–1403.

Hobart, M. A., Herman, B. M., and Langseth, M. G., in press. Heat flow in the Northwest Atlantic Ocean: regional analysis. *J. Geophys. Res.*

Houtz, R., and Ewing, J., 1976. Upper crustal structure as a function of plate age. *J. Geophys. Res.*, 81:2490–2498.

Karato, S., 1983. Physical properties of basalts from Deep Sea Drilling Project Hole 504B, Costa Rica Rift. *In* Cann, J. R., Langseth, M. G., Honnorez, J., Von Herzen, R. P., White, S. M., et al., *Init. Repts. DSDP*, 69: Washington (U.S. Govt. Printing Office), 687–696.

Karato, S., Wilkens, R. H., and Langseth, M. G., 1983. Shipboard physical-properties measurements of basalts from the Costa Rica Rift, Deep Sea Drilling Project Legs 69 and 70. *In* Cann, J. R., Langseth, M. G., Honnorez, J., Von Herzen, R. P., White, S. M., et al., *Init. Repts. DSDP*, 69: Washington (U.S. Govt. Printing Office), 675–682.

Klitgord, K. D., Huestis, S. P., Mudie, J. D., and Parker, R. L., 1975. An analysis of near-bottom magnetic anomalies: Sea-floor spreading and the magnetized layer. *Geophys. J. R. Astron. Soc.*, 43: 387–424.

Klitgord, K. D., and Mudie, J. D., 1974. The Galapagos Spreading Centre: A near-bottom geophysical survey. *Geophys. J. R. Astron. Soc.*, 38:563–586.

Kowsman, R. O., 1973. Coarse components in surface sediments of the Panama Basin, East Equatorial Pacific. *J. Geol.*, 81:473–494.

LaBrecque, J. L., Kent, D. V., and Cande, S. C., 1977. Revised magnetic anomaly time scale for Late Cretaceous and Cenozoic time. *Geology*, 5:330–335.

Laird, N. P., 1969. Anomalous temperature of bottom water in the Panama Basin, *J. Mar. Res.*, 27:355–357.

________, 1971. Panama Basin deep water—properties and circulation. *J. Mar. Res.*, 29:226–234.

Lonsdale, P., 1977a. Deep-tow observations at the Mounts hydrothermal field, Galapagos rift. *Earth Planet, Sci. Lett.*, 36:92–110.

________, 1977b. Inflow of bottom water to the Panama Basin. *Deep-Sea Res.*, 24:1065–1101.

Lonsdale, R., and Klitgord, K. D., 1978. Structure and tectonic history of the eastern Panama Basin. *Geol. Soc. Am. Bull.*, 89: 981–999.

Molnar, P., and Sykes, L. R., 1969, Tectonics of the Caribbean and middle America regions from focal mechanisms and seismicity. *Geol. Soc. Am. Bull.*, 80:1639–1684.

Ninkovich, D., and Shackleton, N. J., 1975. Distribution, stratigraphic position and age of ash layer "L" in the Panama Basin region. *Earth Planet. Sci. Lett.*, 27:20–34.

Ratcliffe, E. H., 1960. The thermal conductivities of ocean sediments. *J. Geophys. Res.*, 65:1535–1541.

Sclater, J. G., and Francheteau, J., 1970. The implications of terrestrial heat flow observations on current tectonic and geochemical models of the crust and upper mantle of the earth. *Geophys. J. R. Astron. Soc.*, 20:509–542.

Searle, R. C., 1983. GLORIA survey over Costa Rica Rift: Sites 501, 504, and 505. *In* Cann, J. R., Langseth, M. G., Honnorez, J., Von Herzen, R. P., White, S. M., et al., *Init. Repts. DSDP*, 69: Washington (U.S. Govt. Printing Office), 217–222.

Stephen, R. A., 1983. The oblique seismic experiment on Deep Sea Drilling Project Leg 70. *In* Cann, J. R., Langseth, M. G., Honnorez, J., Von Herzen, R. P., White, S. M., et al., *Init. Repts. DSDP*, 69: Washington (U.S. Govt. Printing Office), 301–308.

Stephen, R. A., Louden, K. E., and Matthews, D. H., 1980. The oblique seismic experiment on Deep Sea Drilling Project Leg 52. *In* Donnelly, T. W., Francheteau, J., Bryan, W., Robinson, P., Salisbury, M., et al., *Init. Repts. DSDP*, 51, 52, 53, Pt. 1: Washington (U.S. Govt. Printing Office), 301–308.

van Andel, T. H., Heath, G. R., Malfait, B. T., Heinrichs, D. F., and Ewing, J. I., 1971. Tectonics of the Panama Basin, eastern equatorial Pacific. *Geol. Soc. Am. Bull.*, 82:1489–1508.

Vogt, P. R., and de Boer, 1976. Morphology, magnetic anomalies and basalt magnetization at the ends of the Galapagos high-amplitude zones. *Earth Planet. Sci. Lett.*, 33:145–163.

Vogt, P. R., and Johnson, G. L., 1973. Magnetic telechemistry of oceanic crust. *Nature*, 245:373–375.

Von Herzen, R. P., and Maxwell, A. E., 1959. The measurement of thermal conductivity of deep-sea sediments by a needle probe method. *J. Geophys. Res.*, 64:1557–1563.

Wilkens, R. H., and Langseth, M. G., 1983. Physical properties of sediments of the Costa Rica Rift, Deep Sea Drilling Project Sites 504 and 505. *In* Cann, J. R., Langseth, M. G., Honnorez, J., Von Herzen, R. P., White, S. M., et al., *Init. Repts. DSDP*, 69: Washington (U.S. Govt. Printing Office), 659–674.

Williams, D. L., Von Herzen, R. P., Sclater, J. G., and Anderson, R. N., 1974. The Galapagos Spreading Centre: lithospheric cooling and hydrothermal circulation. *Geophys. J. R. Astron. Soc.*, 38: 587–608.

Date of Acceptance: 14 June 1984

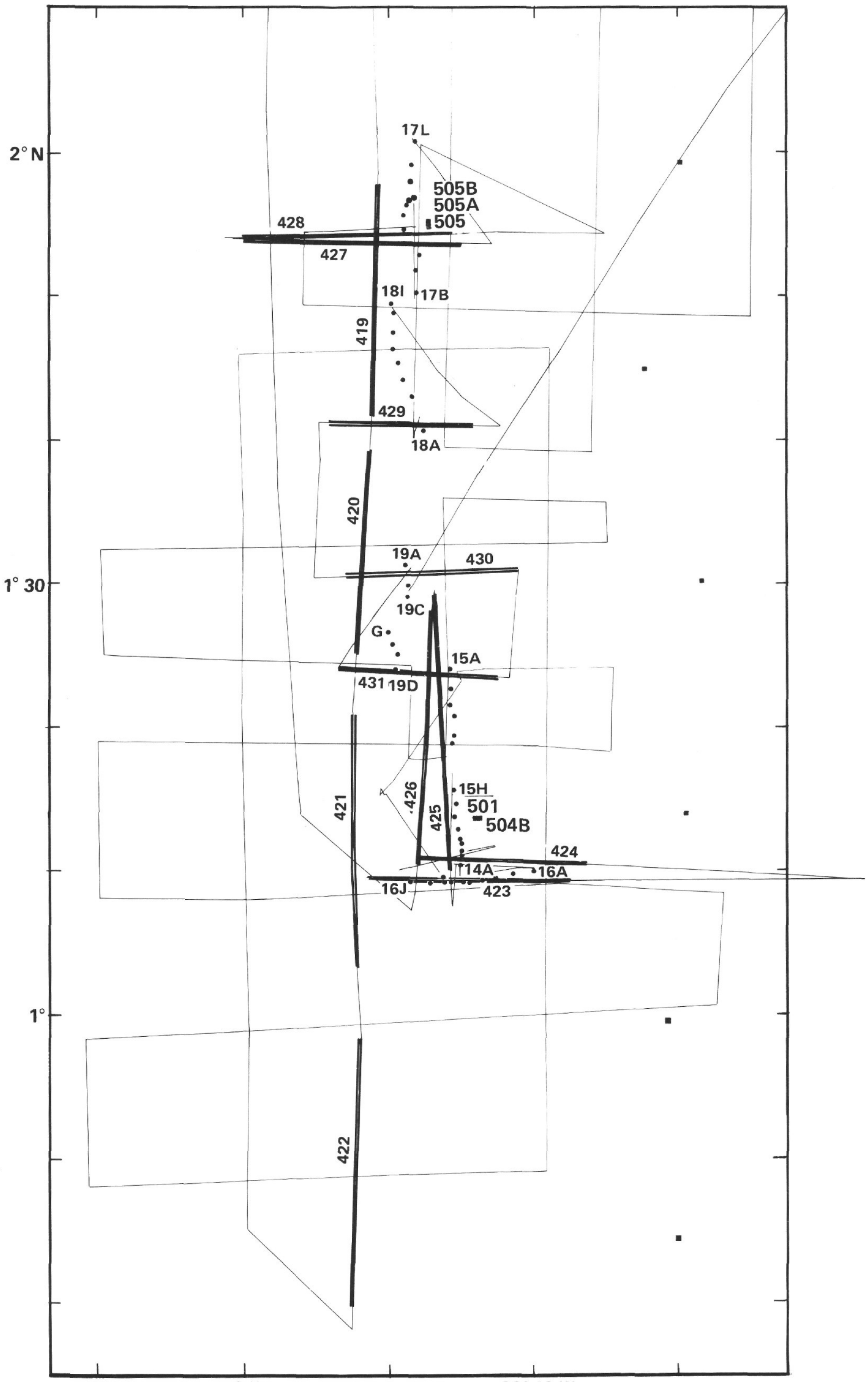

Figure 20. Detailed track chart of *Robert D. Conrad* cruise 21-17 on the flank of the Costa Rica Rift, showing sonobuoy locations.

Table 2. *Conrad* 21-17 sonobuoy stations.

Sonobuoy	Layer	H (s)	Intercept (s)	V_p (km/s)	Thickness (km)	Intercept (s)	V_s (km/s)	Thickness (km)
415	1 water	3.835		1.50	2.56		No shear arrivals	
	2 sed.			(1.60)	0.11			
	3		3.75	4.60	0.96			
	4		4.08	5.75	2.19			
	5		4.66	7.2				
416	1 water	4.28		1.50	2.85		No shear arrivals	
	2 sed.			(1.60)	0.29			
	3		4.28	3.9	0.64			
	4		4.66	5.2?	1.16			
	5		5.09	6.85	2.69			
	6		5.68	8.50				
417	1 water	4.19		1.50	2.79		No shear arrivals	
	2 sed.			(1.60)	0.08			
	3		4.00	4.2	0.87			
	4		4.49	6.6	2.28			
	5		5.00	8.4				
419	1 water	4.59		1.50	3.06		No shear arrivals	
	2 sed.			(1.60)	0.34			
	3		4.46	3.3	0.42			
	4		5.05	5.8	1.06			
	5		5.34	7.15				
420	1 water	4.31		1.50	2.87		No shear arrivals	
	2 sed.			(1.60)	0.20			
	3		4.22	4.0	0.73			
	4		4.63	5.5	1.00			
	5		4.88	6.3	0.94			
	6		5.10	7.0	1.56			
	7		5.41	7.8				
421	1 water	4.60		1.50	3.07			
	2 sed.	0.28		(1.60)	0.17			
	3		4.50	4.25	0.72		(2.80)	0.65
	4		4.86	5.65	0.90	4.53	3.2	0.63
	5		5.07	6.35	1.18	4.77	3.4	1.73
	6		5.35	7.20	2.56	5.83	4.35	
	7		5.80	8.1?				
422	1 water	4.635		1.50	3.09		Shear arrivals very weak	
	2 sed.	0.32		(1.60)	0.32			
	3			(4.50)	0.86			
	4		5.05	6.0	1.68			
	5		5.35	6.65	2.02			
	6		5.75	7.4?				
423	1 water	4.60		1.50	3.07			
	2 sed.			(1.60)	0.34		(1.60)	0.24
	3		4.76	4.70	0.45		(2.80)	0.93
	4		4.90	5.25	0.17	4.74	3.35	1.69
	5		5.04	6.25	2.02	5.43	3.80	
	6		5.77	7.5				

Table 2. (Continued).

Sonobuoy	Layer	H (s)	Intercept (s)	V_p (km/s)	Thickness (km)	Intercept (s)	V_s (km/s)	Thickness (km)
424	1 water	4.51		1.50	3.01			
	2 sed.			(1.60)	0.28		(1.60)	0.28
	3		4.60	4.65	0.52		(2.80)	0.97
	4		4.83	5.80	1.12	4.44	3.05	0.11
	5		5.10	6.75	3.85	4.72	3.40	0.41
	6		5.60	7.3?	1.23	4.87	3.55	2.76
	7		6.17	8.7		6.32	4.67	
425	1 water	4.64		1.50	3.09			
	2 sed.			(1.60)	0.30			
	3		4.81	5.3	0.83		(3.10)	1.48
	4		5.04	6.3	2.49	4.96	3.58	2.37
	5		5.50	7.2		5.82	4.05	
426	1 water	4.63		1.50	3.09			
	2 sed.	0.29		(1.60)	0.34			
	3		4.82	4.95	0.69			
	4		5.10	6.45	1.33		(3.10)	1.86
	5		5.34	7.23	2.63	5.18	3.75	3.23
	6		5.84	8.4		6.69	4.85	
427	1 water	4.60		1.50	3.07		No shear arrivals	
	2 sed.			(1.60)	0.32			
	3		4.78	5.1	0.94			
	4		5.10	6.55	1.33			
	5		5.35	7.40	1.59			
	6		5.61	8.1?				
428	1 water	4.53		1.50	3.02		No shear arrivals	
	2 sed.			(1.60)	0.37			
	3		4.60	3.90	0.40			
	4		4.77	4.35	0.01			
	5		4.98	5.90	0.82			
	6		5.15	6.60				
429	1 water	4.20		1.50	2.80		No shear arrivals	
	2 sed.			(1.60)	0.15			
	3		4.14	4.56	0.61		Velocities corrected for dip	
	4		4.35	5.36	0.28			
	5		4.52	6.53				
430	1 water	4.56		1.50	3.04			
	2 sed.	0.25		(1.60)	0.19			
	3		4.51	4.4	0.83		(3.10)	1.92
	4		4.94	6.4		5.00	3.6	
431	1 water	4.73		1.50	3.15			
	2 sed.			(1.60)	0.17			
	3		4.58	4.0	0.40		(2.26)	0.72
	4		4.88	5.4	0.84	4.69	3.05	0.34
	5		5.15	6.6	1.66	5.02	3.50	
	6		5.37	7.05				

Note: V_p = compressional-wave velocity; V_s = shear-wave velocity.

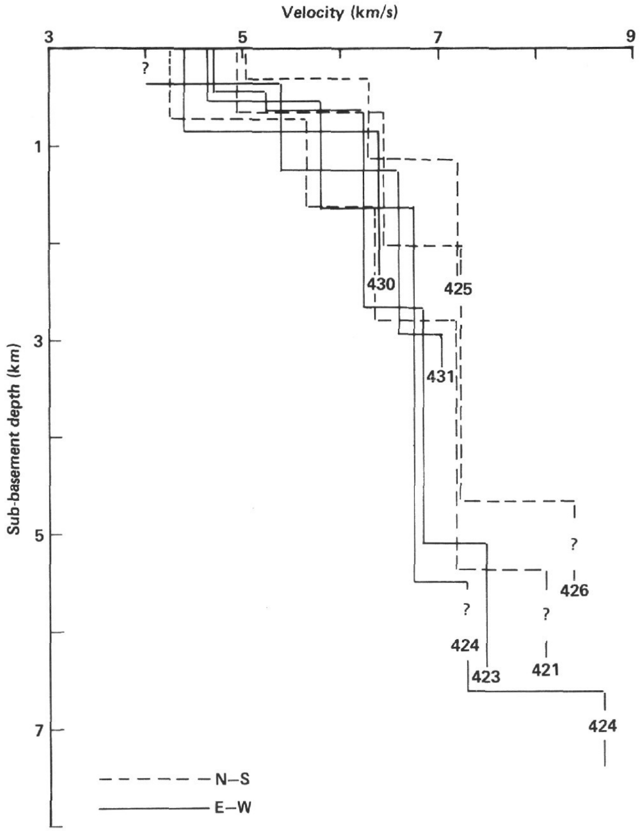

Figure 21. Compressional-wave velocity structure in high-heat-flow area.

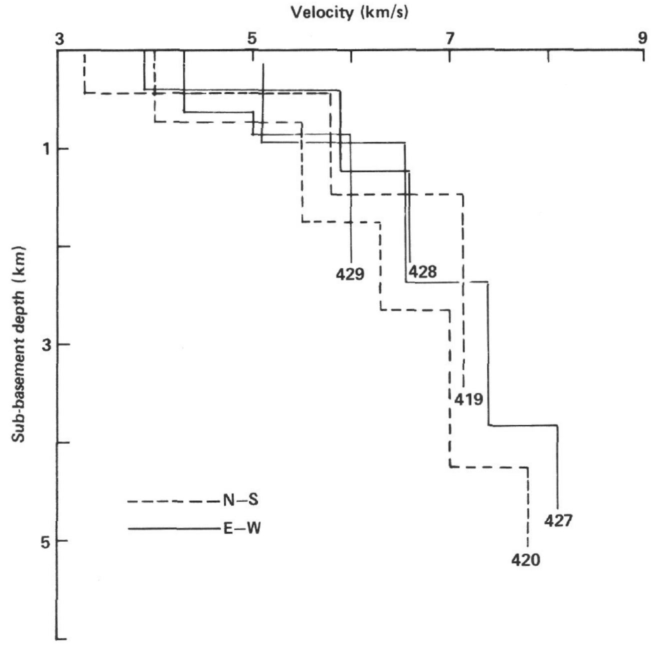

Figure 23. Compressional-wave velocity in low-heat-flow area.

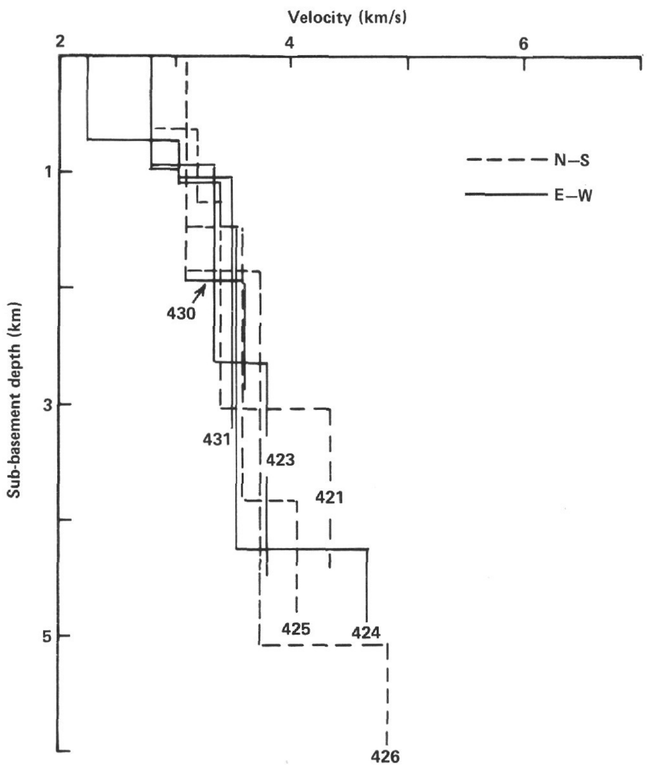

Figure 22. Shear-wave velocity structure in high-heat-flow area.

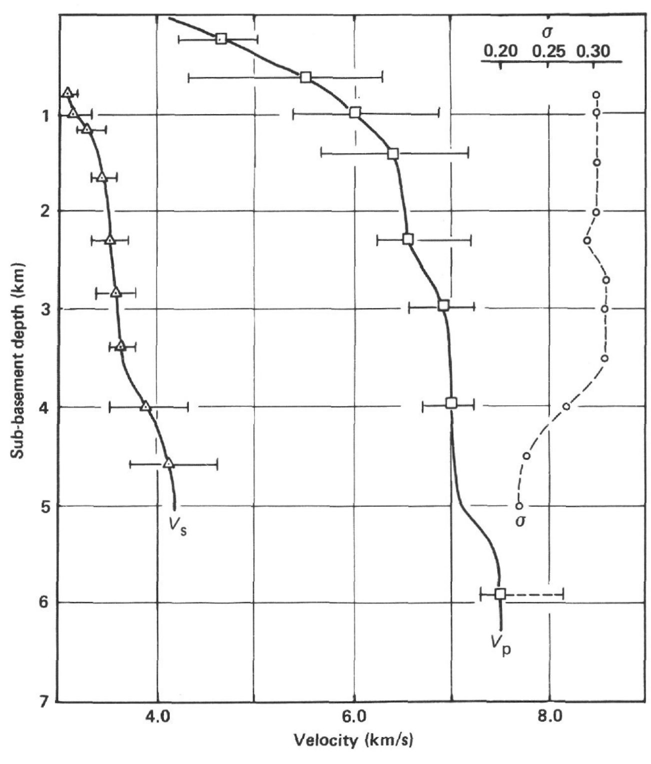

Figure 24. Average compressional- and shear-wave profiles (V_p and V_s, respectively) along with Poisson's ratio (σ) for high-heat-flow area.

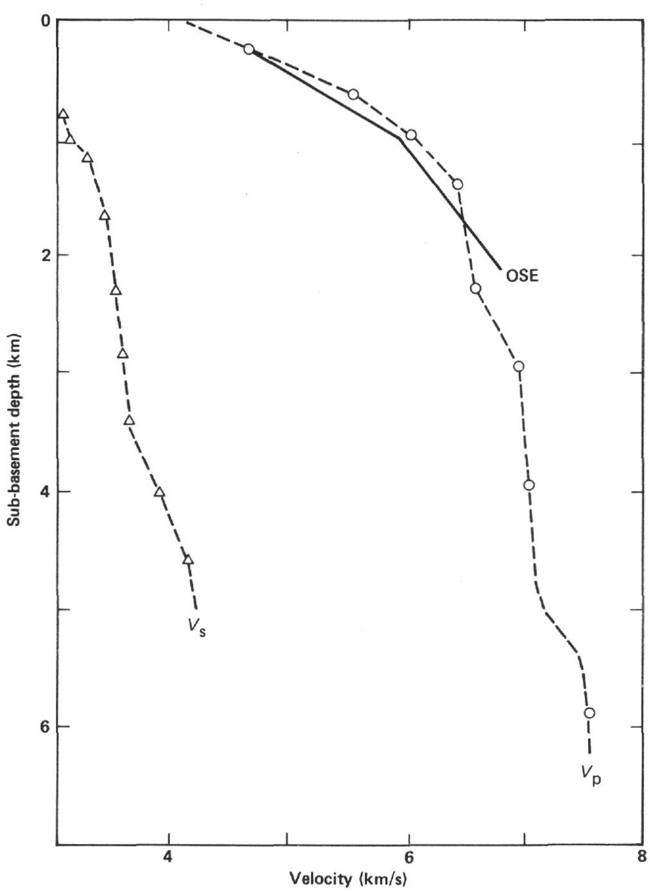

Figure 25. Comparison of the upper part of Figure 24 with results of the Oblique Seismic Experiment (OSE) in Hole 504B (Stephen, 1983).

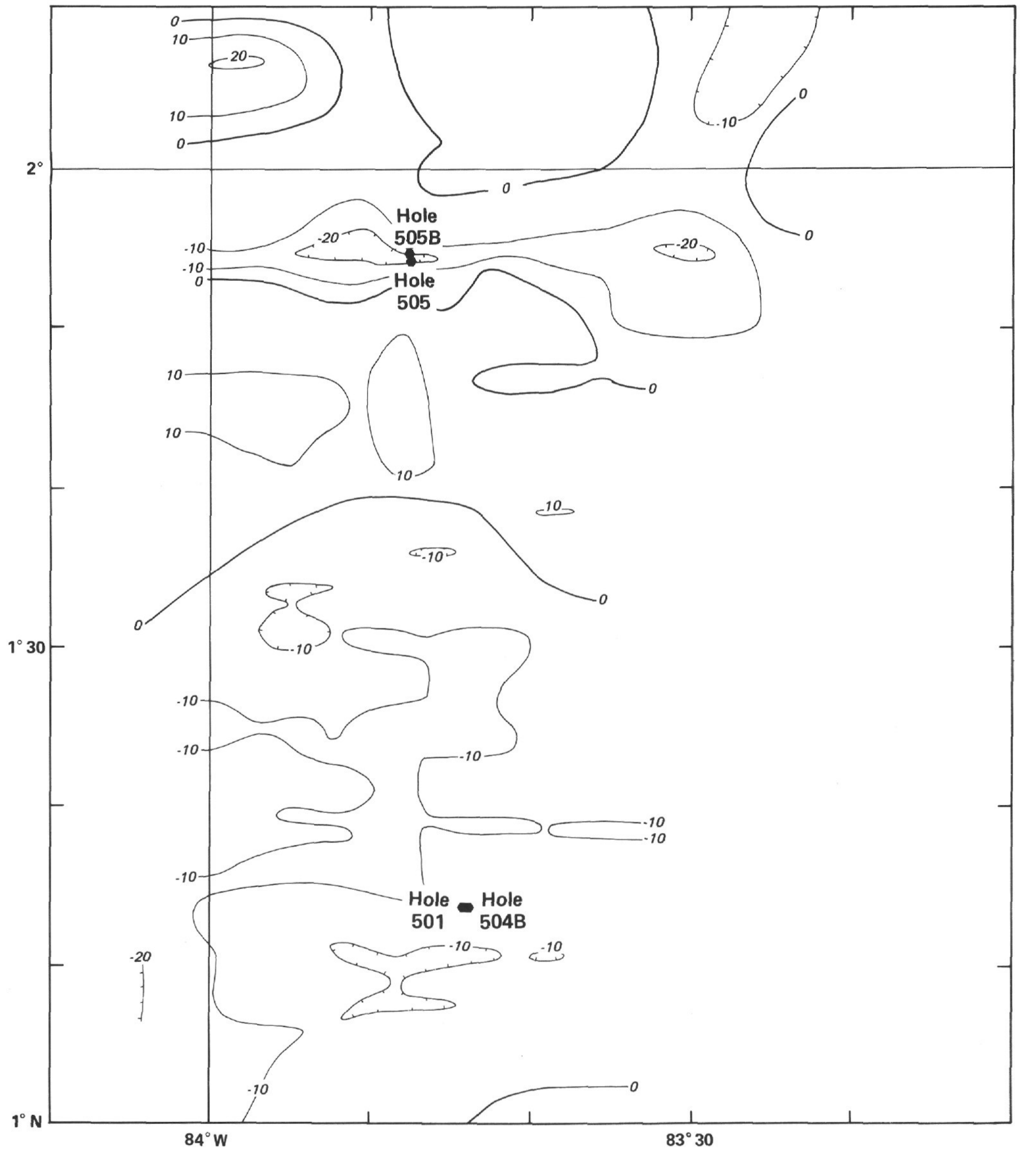

Figure 26. Free-air gravity anomalies (mgals) from the *Conrad* 21-17 survey.